Chapter 9

Groundwater Flow Modeling Techniques

Groundwater is essentially a hidden resource; therefore, studies of groundwater under both natural and artificial boundary conditions have employed modeling techniques. Fortunately, during the past several decades, computer simulation models for analyzing flow and solute transport in groundwater systems have played an increasing role in the evaluation approaches to groundwater development and management.

9.1 WHY DEVELOP GROUNDWATER MODELS?

Alley et al.[1] define groundwater models:

> Groundwater models are an attempt to represent the essential features of the actual groundwater system by means of a mathematical counterpart. The underlying philosophy is that an understanding of the basic laws of physics, chemistry, and biology that describe groundwater flow and transport and an accurate description of the specific system under study will enable a quantitative representation of the cause and effect relationships for that system. Quantitative understanding of cause and effect relationships enables forecasts to be made for any defined set of conditions.

Konikow and Bredehoeft[31] point out that such forecasts, which are usually outside the range of observed conditions, typically are limited by uncertainties due to sparse and inaccurate data, poor definition of stresses acting on the system, and errors in system conceptualization. Even though forecasts of future events using models may be imprecise, they do represent the best available information at a given time that can be used in decision making. Simulation models can be used as learning tools to identify additional data needed in order to better define and understand groundwater systems. These models have the capability to test and quantify the consequences of various errors and uncertainties in the information needed to determine the cause and effect relationships and related model-based forecasts. In the process of forecasting, this model capability may be the most important aspect to define the uncertainties of the forecasts, allowing water managers to evaluate the significance of their decisions. Also this process may allow the evaluation of unexpected consequences of their decisions.

Groundwater modeling has become a very important process in managing groundwater resources. It is interesting to note that each of the classic texts by Walton,[59] Freeze and Cherry,[11] and Todd,[57] dated respectively 1970, 1979, and 1980, had very little material dealing with groundwater modeling using the computer. The past two decades have resulted in tremendous changes in our use of the computer for groundwater management.

9.2 TYPES OF GROUNDWATER MODELS

Todd[57] classified groundwater models as porous media models (sand tank models and transparent models), analog models (viscous fluid models, membrane models, Moire pattern models, thermal models, and blotting paper models), electric analog models (conductive solid models, resistance–capacitance networks, and resistance networks), and digital computer models (finite difference models, finite element models, and hybrid computer models). Prickett[49, 50] provided a detailed list of references on the various models that existed during that time, listing applications of various types of groundwater models, including aquifer features, purpose of the models, and schematic sketches of the models.

A great deal has changed in groundwater modeling since the 1970s, when the numerical (or mathematical) modeling approach was a relatively new field. It was not extensively pursued until the mid-1960s, when digital computers with adequate capacity became generally available (Appel and Bredehoeft).[5] During the 1970s, many articles in the literature, government publications, and books, such as Peaceman,[43] Pinder and Gray,[45] Prickett and Lonnquist,[51] Remson et al.,[54] Rushton and Redshaw,[55] Texas Water Development Board,[56] and Trescott et al.,[58] appeared. Presently, the use of mathematical models is the state-of-the-art in practice for groundwater modeling.

Groundwater models (for the purposes of this book) are physically based mathematical models derived from Darcy's law and the law of conservation of mass.[64] Various established solution techniques based upon either finite difference or finite element approximations, or a combination of both, are available for solving the governing equations of the model. The accuracy of the solutions (model predictions) is dependent upon the reliability of the estimated model parameters and the accuracy of the prescribed boundary conditions.

Groundwater models can be classified in several ways: steady state or transient; confined, unconfined, or a combination of confined and unconfined; one-dimensional, two-dimensional, quasi–three-dimensional, or three-dimensional. They can be solved using *finite difference methods* or *finite element methods* or a combination of these. The major emphasis in this chapter is on the finite difference method.

The finite difference method requires a rectangular element shaped discretization of the aquifer and the finite element method consists of a triangular discretization as illustrated in Figure 9.2.1. The size and shape of the finite elements are arbitrary, typically being triangular or quadrilateral. In fact, the elements can be disordered and nonuniform and should be the smallest where flow is concentrated, such as near a well. Also, it is easy to define the boundaries of

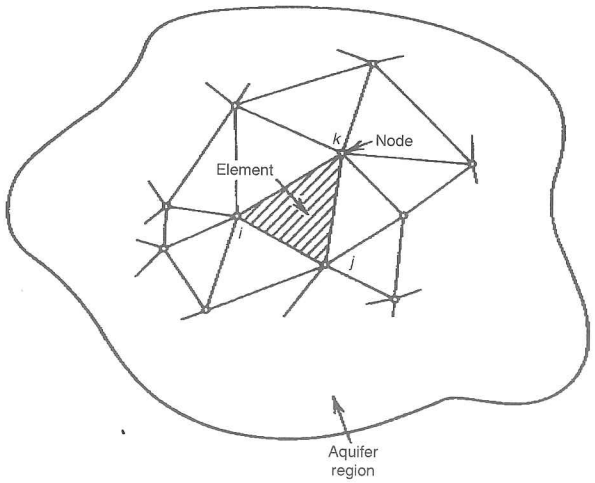

Figure 9.2.1. Example of a triangular finite element within an aquifer (after Prickett[49]).

irregularly shaped aquifers and to ensure that node points coincide with monitoring wells or various types of geographic features. The mathematical basis for finite element methods is more complex than for the finite difference method. Galerkin's method is the most commonly used solution method for the finite element method. Detailed descriptions, while not discussed in this book, of the finite element method can be found elsewhere in the literature.[23, 54, 62]

9.3 STEPS IN THE DEVELOPMENT OF A GROUNDWATER MODEL

Anderson and Woessner[4] presented the following modeling protocol for groundwater modeling:

1. Determine the purpose of the model.
2. Develop a conceptual model.
3. Select the governing equations and computer code.
4. Model design—put the conceptual model into a form suitable for modeling.
5. Calibration—establish that the model can reproduce field-measured heads and flows.
6. Calibration sensitivity analysis—determine the effect of uncertainty on the calibrated model.
7. Model verification—use the calibrated parameter values and stresses to reproduce a second set of field data in order to establish greater confidence in the model.
8. Prediction to quantify the response of the system to future events.
9. Predictive sensitivity analysis to quantify the effect of parameter uncertainty.
10. Presentation of modeling design and results.
11. Post-audit analysis in the future with new field data.
12. Model redesign using insight from the post-audit analysis.

See Hill[25] for more insight on effective model calibration.

9.4 SIMULATION OF TWO-DIMENSIONAL GROUNDWATER SYSTEMS

The first finite difference groundwater models that found fairly widespread usage were developed for two-dimensional (horizontal) flow. These included models such the ones developed by Prickett and Lonnquist,[51] Trescott et al.,[58] and the Texas Water Development Board.[56] Even though the use of these models has been superceded by the U.S. Geological Survey MODFLOW model (which can be used for either two- or three-dimensional modeling), it is worthwhile to describe the two-dimensional framework as a precursor to a description of the more complicated three-dimensional models.

9.4.1 Governing Equations

Darcy's law relates the Darcy flux v with dimension (L/T) to the rate of headloss per unit length of porous medium $\partial h / \partial l$, as discussed in Chapter 3. The negative sign indicates that the total head is decreasing in the direction of flow because of friction. This law applies to a cross section of porous medium, which is large compared to the cross section of individual pores and grains of the medium. At this scale, Darcy's law describes a steady uniform flow of constant velocity, in which the net force on any fluid element is zero. For unconfined saturated flow, the two forces are gravity and friction. Darcy's law (Equation 3.1.5) can also be expressed in terms of the transmissivity for confined conditions as

$$v = -\frac{T}{b}\frac{\partial h}{\partial l} \tag{9.4.1}$$

or for unconfined conditions as

$$v = -\frac{T}{h}\frac{\partial h}{\partial l} \tag{9.4.2}$$

where b is the thickness of the confined aquifer and h is the saturated thickness of the unconfined aquifer.

Considering two-dimensional (horizontal) flow, a general flow equation can be derived by considering flow through a rectangular element (control volume), as shown in Figure 9.4.1. The flow components ($q = Av$) for the four sides of the element are expressed using Darcy's law where $A = \Delta x \cdot h$ for unconfined conditions and $A = \Delta x \cdot b$ for confined conditions so that

$$q_1 = -T_{x_{i-1,j}} \Delta y_j \left(\frac{\partial h}{\partial x}\right)_1 \tag{9.4.3a}$$

$$q_2 = -T_{x_{i,j}} \Delta y_j \left(\frac{\partial h}{\partial x}\right)_2 \tag{9.4.3b}$$

$$q_3 = -T_{y_{i,j+1}} \Delta x_i \left(\frac{\partial h}{\partial y}\right)_3 \tag{9.4.3c}$$

$$q_4 = -T_{y_{i,j}} \Delta x_i \left(\frac{\partial h}{\partial y}\right)_4 \tag{9.4.3d}$$

where $T_{x_{i,j}}$ is the transmissivity in the x flow direction from element (i, j) to element $(i + 1, j)$. The terms $(\partial h/\partial x)_1$, $(\partial h/\partial x)_2$, . . . , define the hydraulic gradients at the element sides 1, 2, ...

The rate at which water is stored or released in the element over time is

$$q_5 = S_{i,j} \Delta x_i \Delta y_i \frac{\partial h}{\partial t} \tag{9.4.4}$$

in which $S_{i,j}$ is the storage coefficient for element (i, j). In addition, the flow rate q_6 for constant net withdrawal or recharge from the element over time interval Δt is considered as

$$q_6 = q_{i,j,t} \tag{9.4.5}$$

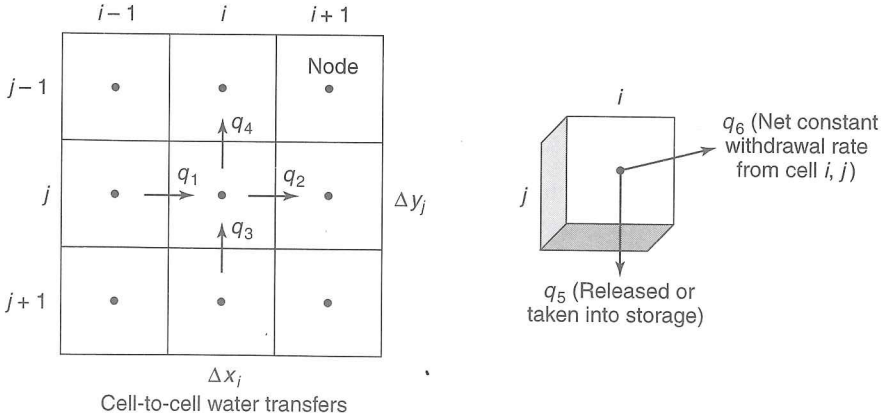

Figure 9.4.1. Finite difference grid showing the control volume for an element of a two-dimensional (horizontal) flow. The node within each grid (cell) is the point where the head is calculated.

in which $q_{i,j,t}$ has a positive value for pumping, whereas it has a negative value for recharge.

By continuity the flow into and out of a grid or cell is

$$q_1 - q_2 + q_3 - q_4 = q_5 + q_6 \tag{9.4.6}$$

Substituting in Equations 9.4.3 and 9.4.5 gives

$$\begin{aligned} &-T_{x_{i-1,j}} \Delta y_j \left(\frac{\partial h}{\partial x}\right)_1 + T_{x_{i,j}} \Delta y_j \left(\frac{\partial h}{\partial x}\right)_2 - T_{y_{i,j+1}} \Delta x_i \left(\frac{\partial h}{\partial y}\right)_3 + T_{y_{i,j}} \Delta x_i \left(\frac{\partial h}{\partial y}\right)_4 \\ &= S_{i,j} \Delta x_i \Delta y_i \frac{\partial h}{\partial t} + q_{i,j,t} \end{aligned} \tag{9.4.7}$$

Dividing Equation 9.4.7 by $\Delta x\, \Delta y$ and simplifying for constant transmissivities in the x and y directions yields

$$-T_x \left[\frac{\left(\frac{\partial h}{\partial x}\right)_1 - \left(\frac{\partial h}{\partial x}\right)_2}{\Delta x_i} \right] - T_y \left[\frac{\left(\frac{\partial h}{\partial y}\right)_3 - \left(\frac{\partial h}{\partial y}\right)_4}{\Delta y_j} \right] = S_{i,j} \frac{\partial h}{\partial t} + \frac{q_{i,j,t}}{\Delta x_i \Delta y_j} \tag{9.4.8}$$

For Δx and Δy infinitesimally small, the terms in brackets [ ] become second derivatives of h. Then Equation 9.4.8 reduces to

$$T_x \frac{\partial^2 h}{\partial x^2} + T_y \frac{\partial^2 h}{\partial y^2} = S \frac{\partial h}{\partial t} + W \tag{9.4.9}$$

which is the general partial differential equation for unsteady flow in the horizontal direction in which $W = q_{i,j,t}/\Delta x_i \Delta y_j$ is a sink term with dimensions (L/T).

In the more general case for unsteady, two-dimensional heterogeneous anisotropic flow, Equation 9.4.9 is expressed as

$$\frac{\partial}{\partial x}\left(T_x \frac{\partial h}{\partial x}\right) + \frac{\partial}{\partial y}\left(T_y \frac{\partial h}{\partial y}\right) = S \frac{\partial h}{\partial t} + W \tag{9.4.10a}$$

or more simply

$$\frac{\partial}{\partial x_i}\left(T_{i,j} \frac{\partial h}{\partial x_j}\right) = S \frac{\partial h}{\partial t} + W \quad i, j = 1, 2 \tag{9.4.10b}$$

9.4.2 Finite Difference Equations

The partial derivative expressions for Darcy's law, (Equations 9.4.3a–d), can be expressed in finite difference form for time t in Equation 9.4.7 using

$$\left(\frac{\partial h}{\partial x}\right)_1 = \left(\frac{h_{i-1,j,t} - h_{i,j,t}}{\Delta x_i}\right) \tag{9.4.11a}$$

$$\left(\frac{\partial h}{\partial x}\right)_2 = \left(\frac{h_{i,j,t} - h_{i+1,j,t}}{\Delta x_i}\right) \tag{9.4.11b}$$

$$\left(\frac{\partial h}{\partial y}\right)_3 = \left(\frac{h_{i,j+1,t} - h_{i,j,t}}{\Delta y_j}\right) \tag{9.4.11c}$$

$$\left(\frac{\partial h}{\partial y}\right)_4 = \left(\frac{h_{i,j,t} - h_{i,j-1,t}}{\Delta y_j}\right) \tag{9.4.11d}$$

and the time derivative in Equation 9.4.10 is

$$\frac{\partial h}{\partial t} = \left(\frac{h_{i,j,t} - h_{i,j,t-1}}{\Delta t}\right) \tag{9.4.12}$$

Substituting Equations 9.4.11 and 9.4.12 into Equation 9.4.7 yields

$$\begin{aligned} &-T_{x_{i-1,j}} \Delta y_j \left(\frac{h_{i-1,j,t} - h_{i,j,t}}{\Delta x_i}\right) + T_{x_{i,j}} \Delta y_j \left(\frac{h_{i,j,t} - h_{i+1,j,t}}{\Delta x_i}\right) \\ &-T_{y_{i,j+1}} \Delta x_i \left(\frac{h_{i,j+1,t} - h_{i,j,t}}{\Delta y_j}\right) + T_{y_{i,j}} \Delta x_i \left(\frac{h_{i,j,t} - h_{i,j-1,t}}{\Delta y_j}\right) \\ &-S_{i,j} \Delta x_i \Delta y_j \left(\frac{h_{i,j,t} - h_{i,j,t-1}}{\Delta t}\right) - q_{i,j,t} = 0 \end{aligned} \tag{9.4.13}$$

which can be further simplified to

$$\begin{aligned} &A_{i,j} h_{i,j,t} + B_{i,j} h_{i-1,j,t} + C_{i,j} h_{i+1,j,t} + D_{i,j} h_{i,j+1,t} + \\ &E_{i,j} h_{i,j-1,t} + F_{i,j,t} = 0 \end{aligned} \tag{9.4.14}$$

where

$$A_{i,j} = \left[T_{x_{i-1,j}} \frac{\Delta y_j}{\Delta x_i} + T_{x_{i,j}} \frac{\Delta y_j}{\Delta x_i} + T_{y_{i,j+1}} \frac{\Delta x_i}{\Delta y_j} + T_{y_{i,j}} \frac{\Delta x_i}{\Delta y_j} - S_{i,j} \frac{\Delta x_i \Delta y_j}{\Delta t} \right] \tag{9.4.15a}$$

$$B_{i,j} = -T_{x_{i-1,j}} \frac{\Delta y_j}{\Delta x_i} \tag{9.4.15b}$$

$$C_{i,j} = -T_{x_{i,j}} \frac{\Delta y_j}{\Delta x_i} \tag{9.4.15c}$$

$$D_{i,j} = -T_{y_{i,j+1}} \frac{\Delta x_i}{\Delta y_j} \tag{9.4.15d}$$

$$E_{i,j} = -T_{y_{i,j}} \frac{\Delta x_i}{\Delta y_j} \tag{9.4.15e}$$

$$F_{i,j,t} = -S_{i,j} \frac{\Delta x_i \Delta y_j}{\left(\frac{h_{i,j,t} - h_{i,j,t-1}}{\Delta t}\right)} - q_{i,j,t} \tag{9.4.15f}$$

The coefficients $A_{i,j}$, $B_{i,j}$, $C_{i,j}$, $D_{i,j}$, $E_{i,j}$, and $F_{i,j,t}$ are linear functions of the thickness of cell (i, j) and the thickness of one of the adjacent cells. For artesian conditions, this thickness is a known constant, so if cell (i, j) and its neighbors are artesian, Equation 9.4.14 is linear for all t. For unconfined (water table) conditions, the thickness of cell (i, j) is $h_{i,j,t} - BOT_{i,j}$, where

$BOT_{i,j}$ is the average elevation of the bottom of the aquifer for cell (i, j). Then for unconfined conditions, Equation 9.4.14 involves products of heads and is nonlinear in terms of the heads.

9.4.3 Solution

An *iterative alternating direction implicit (IADI) procedure* can be used to solve the set of equations. The IADI procedure involves reducing a large set of equations to several smaller sets of equations. A smaller set of equations is generated by writing Equation 9.4.14 for each cell or element in a column but assuming that the heads for the nodes on the adjacent columns are known. The unknowns in this set of equations are the heads for the nodes along the column. The heads for the nodes along adjoining columns are not considered unknowns. This set of equations is solved by Gauss elimination and the process is repeated until each column is treated. The next step is to develop a set of equations along each row, assuming the heads for the nodes along adjoining rows are known. The set of equations for each row is solved and the process is repeated for each row in the finite difference grid.

9.4.4 Case Study

Once the sets of equations for the columns and the sets of equations for the row have been solved, one "iteration" has been completed. The iteration process is repeated until the procedure converges. Once convergence is accomplished, the terms $h_{i,j}$ represent the heads at the end of the time step. These heads are used as the beginning heads for the following time step. For a more detailed discussion of the IADI procedure, see references 44, 51, or 62. Two-dimensional finite difference models for groundwater flow are by Prickett and Lonnquist[51] and by Trescott et al.[58]

Two studies utilizing a two-dimensional finite difference groundwater model have been made of the Edwards (Balcones Fault Zone) Aquifer. First, this aquifer has been modeled using the GWSIM groundwater simulation model developed by the Texas Water Development Board.[56] GWSIM is a finite difference simulation model that uses the IADI method similar to the model by Prickett and Lonnquist.[51] The finite difference grid for the Edwards Aquifer is shown in Figure 9.4.2, which has 856 active cells to describe the aquifer. Second, Wanakule[61] has modeled a smaller portion of the Edwards aquifer called the Barton Springs—Edwards Aquifer in Austin, Texas. This application used a finite difference grid system (Figure 9.4.3) containing 330 cells whose dimensions varied from 0.379×0.283 mi^2 to 0.95×1.51 mi^2.

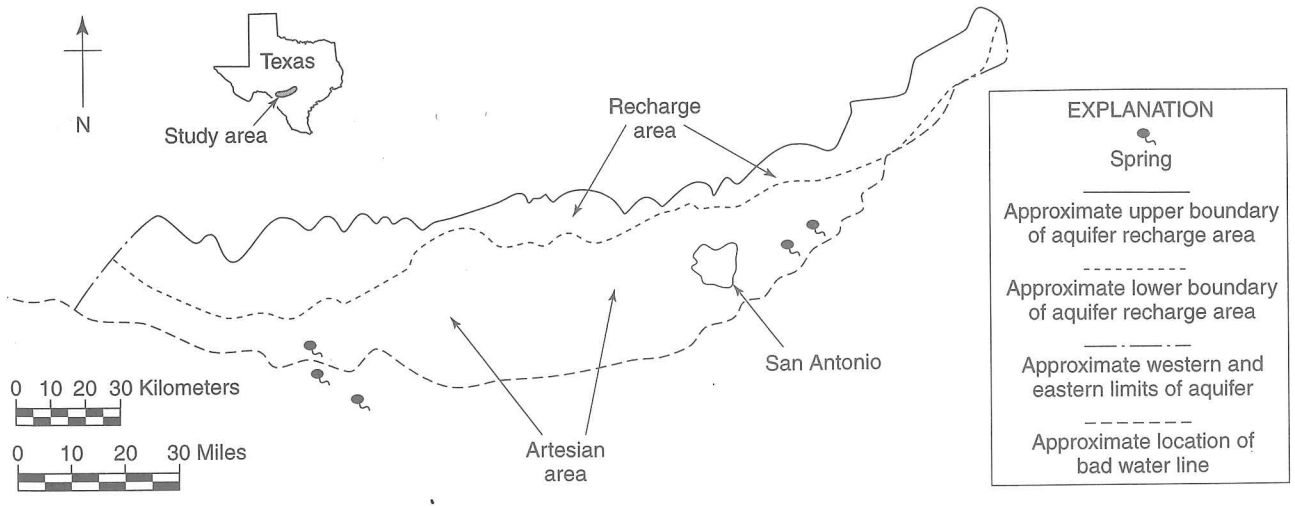

Figure 9.4.2a. Edwards (Balcones Fault Zone) Aquifer, San Antonio, TX, region.[56]

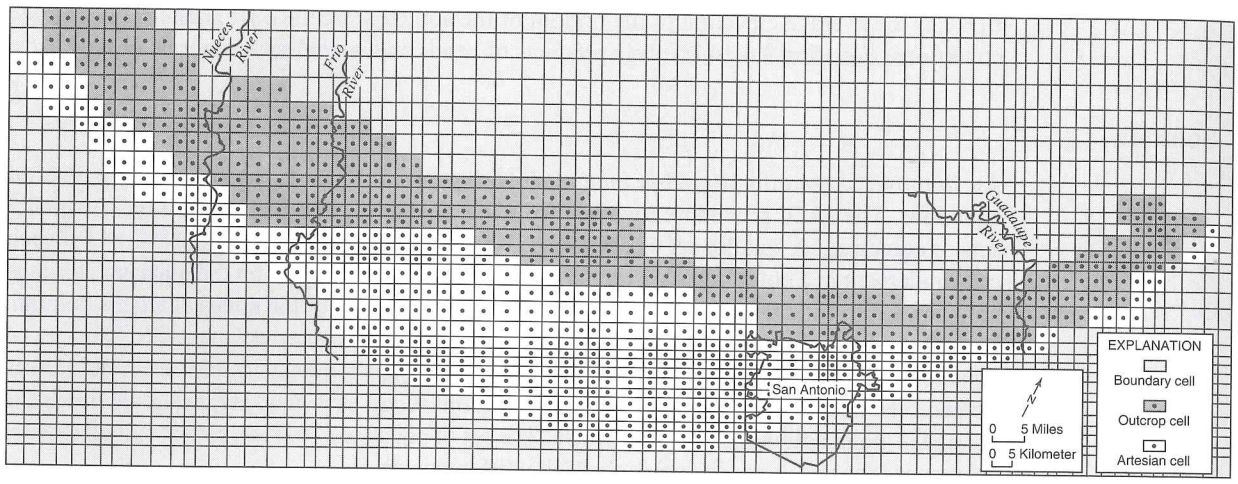

Figure 9.4.2b. Cell map used for the digital computer model of the Edwards (Balcones Fault Zone) Aquifer (after Klempt et al.[30]).

The above two case studies are for the purposes of illustrating the two-dimensional finite difference method for horizontal flows. The present day modeling of the Edwards Aquifer is being done using the MODFLOW model that is introduced in the following sections of this chapter.

9.5 THREE-DIMENSIONAL GROUNDWATER FLOW MODEL

9.5.1 Derivation of Finite Difference Equations

The partial differential equation for transient three-dimensional groundwater flow in a heterogeneous and anisotropic medium (provided the principal axes of hydraulic conductivity are aligned with the coordinate directions), for a confined or unconfined aquifer, is expressed as

$$\frac{\partial}{\partial x}\left(K_{xx}\frac{\partial h}{\partial x}\right)+\frac{\partial}{\partial y}\left(K_{yy}\frac{\partial h}{\partial y}\right)+\frac{\partial}{\partial z}\left(K_{zz}\frac{\partial h}{\partial z}\right)-W=S_s\frac{\partial h}{\partial t} \tag{9.5.1}$$

where K_{xx}, K_{yy}, and K_{zz} are the hydraulic conductivities along the x, y, and z coordinate axes parallel to the major axes of hydraulic conductivities; h is the potentiometric head; W is a volumetric flux per unit volume representing sources (W is negative) and/or sinks (W is positive) of water; S_s is the specific storage of the porous medium; and t is time. K_{xx}, K_{yy}, K_{zz}, and S_s are functions of space (x, y, z) and W is a function of space and time (x, y, z, t).

Equation 9.5.1, together with specification of flow and/or head conditions at the boundaries of an aquifer system and specification of initial head conditions, constitutes a mathematical representation of a groundwater flow system. The solution of Equation 9.5.1 requires the use of a numerical method such as the finite difference method. The application of finite differences replaces the continuous system described by Equation 9.5.1 with a finite set of discrete points in space and time, such that the partial derivatives are replaced by terms calculated from the head differences calculated at these points. A system of simultaneous linear algebraic difference equations results from this process, which is solved for the heads at specific points and times that constitute the approximation to the time-varying head distribution.

Figure 9.5.1 illustrates a three-dimensional hypothetical aquifer system discretized into a mesh of blocks called *cells*, described by rows, columns, and layers. The hypothetical system is discretized into five rows, nine columns, and five layers. An i, j, k indexing system is used

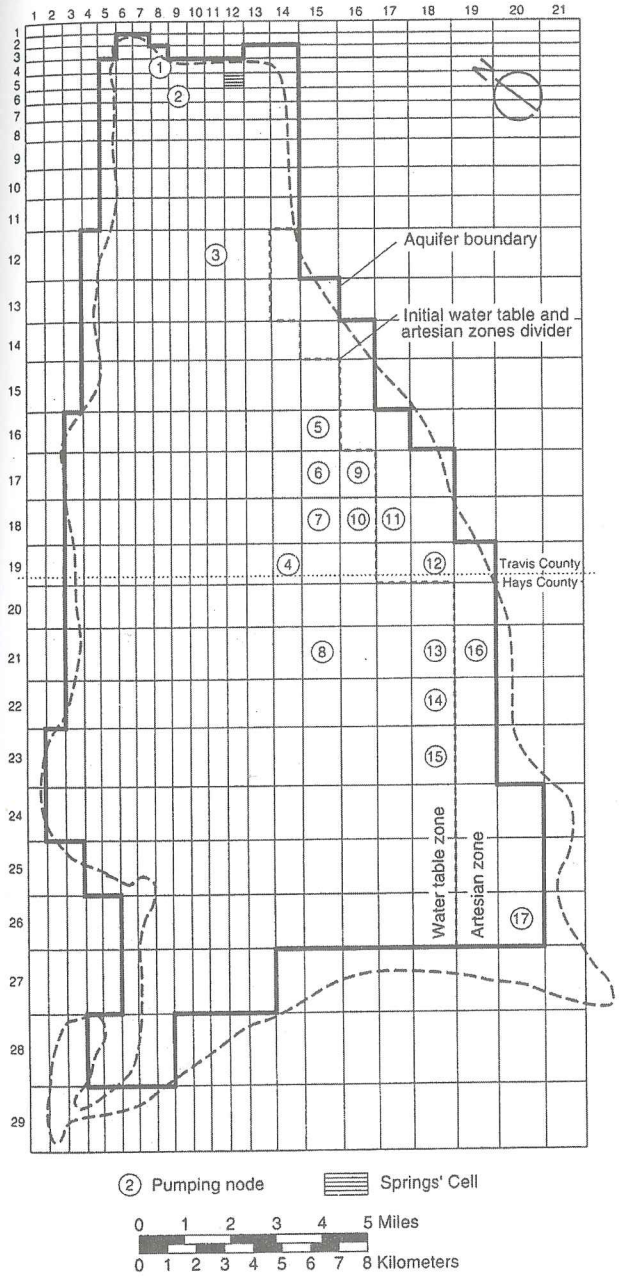

Figure 9.4.3. Pumping locations used in Barton Springs–Edwards Aquifer model (after Wanakule[61]).

to reference the cells. Layers generally refer to horizontal geohydrologic units or intervals, so that the k index denotes changes along the vertical (z-direction in Cartesian coordinates). The layers are numbered from the top down so that an increment in the k index corresponds to a decrease in elevation. Rows are considered parallel to the x axis and columns are parallel to the x axis.

A *node* is a point within each cell (grid) where the head is calculated. Figure 9.5.2 illustrates block-centered and point-centered grid systems. Whichever grid system is used, the

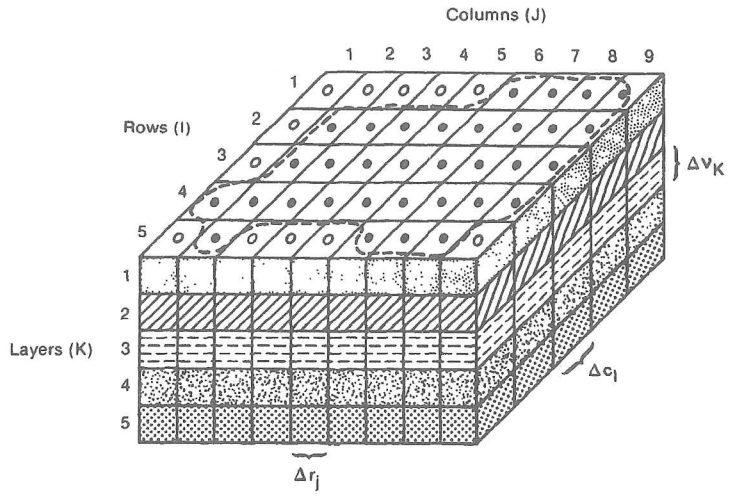

---- Aquifer boundary

• Active cell

0 Inactive cell

Δr_J Dimension of cell along the row direction. Subscript (J) indicates the number of the column.

Δc_I Dimension of cell along the column direction. Subscript (I) indicates the number of the row.

Δv_K Dimension of cell along the vertical direction. Subscript (K) indicates the number of the layer.

Figure 9.5.1. A discretized hypothetical aquifer system (McDonald and Harbaugh[39]).

spacing of nodes should be selected so that the hydraulic properties are generally uniform over the extent of the cell. The finite difference equations developed herein are applicable for either grid system. Figure 9.5.3 illustrates cell (i, j, k) and the six adjacent cells that are used to derive the finite difference equation for the cell.

Figure 9.5.4 illustrates the flow into cell (i, j, k) from cell $(i, j-1, k)$. The effective hydraulic conductivity for the entire region between the nodes is denoted as $KR_{i,j-1/2,k}$. The subscript $j - 1/2$ does not relate to a specific point between the nodes but is used to relate to the region from cell $(i, j-1, k)$ to cell (i, j, k). The effective hydraulic conductivity is computed as the harmonic mean, so that for flow into cell (i, j, k) from cell $(i, j-1, k)$, the *effective hydraulic conductivity* is

$$KY_{i-1/2,j,k} = \frac{(\Delta y_{i-1} + \Delta y_i)/2}{\left(\dfrac{\Delta y_{i-1}/2}{KY_{i-1,j,k}} + \dfrac{\Delta y_i/2}{KY_{i,j,k}}\right)} = \frac{KY_{i-1,j,k}KY_{i,j,k}(\Delta y_{i-1} + \Delta y_i)}{KY_{i,j,k}\Delta y_{i-1} + KY_{i-1,j,k}\Delta y_i} \tag{9.5.2}$$

If Δy is constant, then Equation 9.5.2 is expressed as

$$KY_{i-1/2,j,k} = \frac{2KY_{i,j,k}KY_{i-1,j,k}}{KY_{i,j,k} + KY_{i-1,j,k}} \tag{9.5.3}$$

Flows are considered positive if they are entering cell (i, j, k) and the negative sign incorporated into Darcy's law is dropped from all terms. The flow into cell (i, j, k) from cell $(i, j-1, k)$ is expressed by Darcy's law as (McDonald and Harbaugh[39])

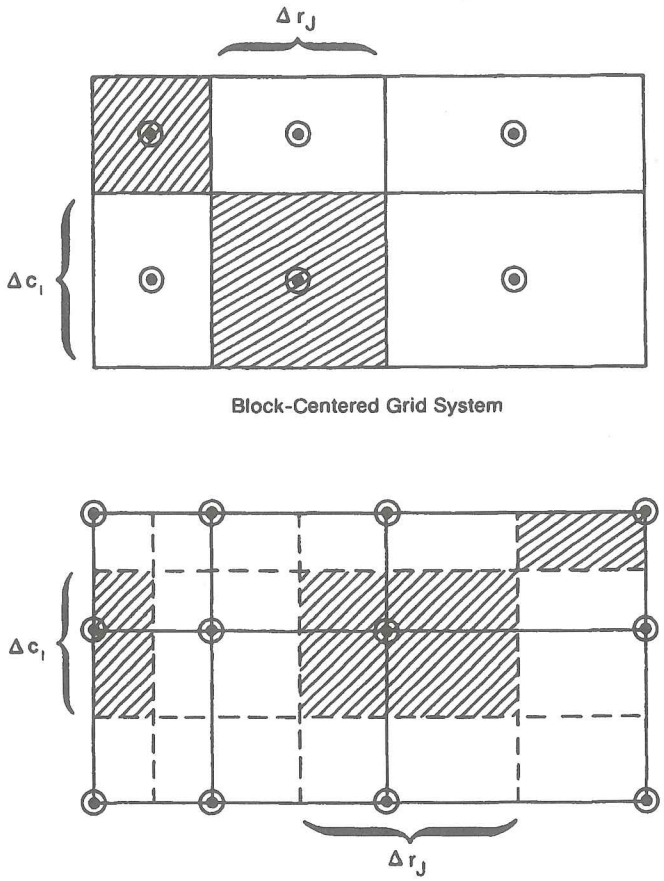

Figure 9.5.2. Grids showing the difference between block-centered and point-centered grids (McDonald and Harbaugh[39]).

$$q_{i,j-1/2,k} = \mathrm{KY}_{i,j-1/2,k}\Delta x_i \Delta z_k \left(\frac{h_{i,j-1,k} - h_{i,j,k}}{\Delta y_{j-1/2}} \right) \tag{9.5.4}$$

where $q_{i,j-1/2,k}$ is the volumetric fluid discharge through the face between cell (i, $j-1$, k) and cell (i, j, k); $h_{i,j,k}$ and $h_{i,j-1,k}$ are the heads at the respective nodes; $\Delta x_i \Delta z_k$ is the area of the cell face normal to the row direction; and $\Delta y_{j-1/2}$ is the distance between nodes (i, j, k) and (i, $j-1$, k). Equation 9.5.4 defines the flow for a one-dimensional steady-state flow through a block of aquifer extending from node (i, $j-1$, k) to node (i, j, k), and having cross-sectional area $\Delta x_i \Delta z_k$.

Darcy's law is applied in a similar manner to describe the flow through the remaining five sides of cell (i, j, k) to obtain the following (McDonald and Harbaugh[39]):

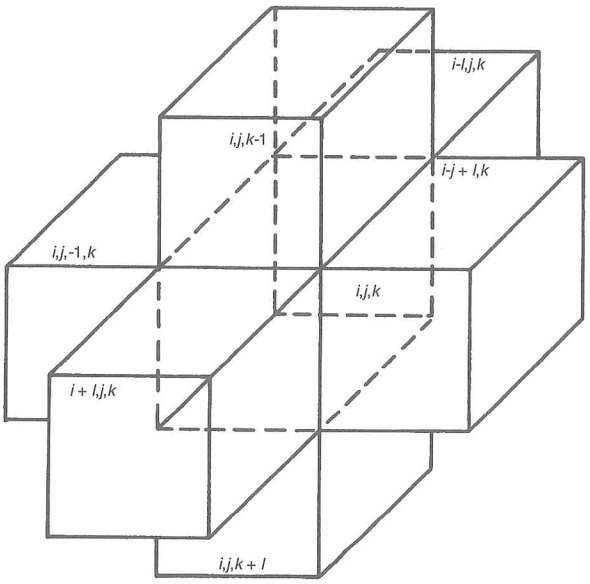

Figure 9.5.3. Cell (i, j, k) and indices for the six adjacent cells (McDonald and Harbaugh[39]).

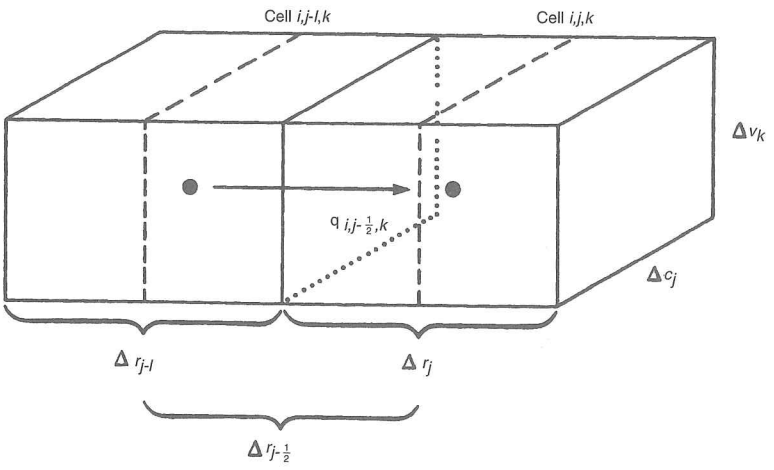

Figure 9.5.4. Flow into cell (i, j, k) from cell $(i, j - 1, k)$ (McDonald and Harbaugh[39]).

Flow cell (i, j, k) to cell $(i, j + 1, k)$

$$q_{i,j+1/2,k} = \mathrm{KY}_{i,j+1/2,k}\Delta x_i \Delta z_k \left(\frac{h_{i,j+1,k} - h_{i,j,k}}{\Delta y_{j+1/2}} \right) \tag{9.5.5}$$

Flow cell (i, j, k) to cell $(i + 1, j, k)$

$$q_{i+1/2,j,k} = \mathrm{KX}_{i+1/2,j,k}\Delta y_j \Delta z_k \left(\frac{h_{i+1,j,k} - h_{i,j,k}}{\Delta x_{i+1/2}} \right) \tag{9.5.6}$$

Flow cell $(i - 1, j, k)$ to cell (i, j, k)

$$q_{i-1/2,j,k} = \mathrm{KX}_{i-1/2,j,k}\Delta y_j \Delta z_k \left(\frac{h_{i-1,j,k} - h_{i,j,k}}{\Delta x_{i-1/2}} \right) \tag{9.5.7}$$

Flow cell (i, j, k) to cell $(i, j, k + 1)$

$$q_{i,j,k+1/2} = \mathrm{KZ}_{i,j,k+1/2}\Delta y_j \Delta x_i \left(\frac{h_{i,j,k+1} - h_{i,j,k}}{\Delta z_{k+1/2}} \right) \tag{9.5.8}$$

Flow cell $(i, j, k - 1)$ to cell (i, j, k)

$$q_{i,j,k-1/2} = \mathrm{KZ}_{i,j,k-1/2}\Delta y_j \Delta x_i \left(\frac{h_{i,j,k-1} - h_{i,j,k}}{\Delta z_{k-1/2}} \right) \tag{9.5.9}$$

Equations 9.5.4 through 9.5.9 describe the steady-state, one-dimensional flow through each side of cell (i, j, k) in terms of the heads, grid dimensions, and hydraulic conductivity. The notation can be simplified by defining a constant referred to as the *hydraulic conductance* or the *conductance* by combining the grid dimensions and hydraulic conductivity. *Conductance* is the product of the effective hydraulic conductivity and cross-sectional area of flow divided by the length of the flow path (distance between nodes). The hydraulic conductance $\mathrm{CY}_{i,j-1/2,k}$ in row i and layer k between nodes $(i, j - 1, k)$ and (i, j, k) is

$$\mathrm{CY}_{i,j-1/2,k} = \mathrm{KY}_{i,j-1/2,k}\, \Delta x_i\, \Delta z_k / \Delta y_{j-1/2} \tag{9.5.10}$$

where $\mathrm{CY}_{i,j-1/2,k}$ is the conductance in row i and layer k between nodes $(i, j-1, k)$ and (i, j, k) [L^2/T].

Equations 9.5.4 through 9.5.9 are expressed with the conductance as

$$q_{i,j-1/2,k} = \mathrm{CY}_{i,j-1/2,k}\,(h_{i,j-1,k} - h_{i,j,k}) \tag{9.5.11}$$

$$q_{i,j+1/2,k} = \mathrm{CY}_{i,j+1/2,k}\,(h_{i,j+1,k} - h_{i,j,k}) \tag{9.5.12}$$

$$q_{i-1/2,j,k} = \mathrm{CX}_{i-1/2,j,k}\,(h_{i-1,j,k} - h_{i,j,k}) \tag{9.5.13}$$

$$q_{i+1/2,j,k} = \mathrm{CX}_{i+1/2,j,k}\,(h_{i+1,j,k} - h_{i,j,k}) \tag{9.5.14}$$

$$q_{i,j,k-1/2} = \mathrm{CZ}_{i,j,k-1/2}\,(h_{i,j,k-1} - h_{i,j,k}) \tag{9.5.15}$$

$$q_{i,j,k+1/2} = \mathrm{CZ}_{i,j,k+1/2}\,(h_{i,j,k+1} - h_{i,j,k}) \tag{9.5.16}$$

The flows from features or processes external to the aquifer, such as streams, drains, areal recharge, evapotranspiration, or wells, are described through additional terms. These flows may be dependent on the head in the receiving cell but independent of all other heads in the aquifer, or they may be entirely independent of head in the receiving cell.

The rate at which water is stored or released in the cell, $\Delta V/\Delta t$ over time Δt, is

$$\frac{\Delta V}{\Delta t} = \mathrm{SS}_{i,j,k}\Delta x_i \Delta y_j \Delta z_k \frac{\Delta h_{i,j,k}}{\Delta t} \tag{9.5.17}$$

where $\mathrm{SS}_{i,j,k}$ is the specific storage of cell (i, j, k); $\Delta h_{i,j,k}/\Delta t$ is the finite difference approximation for the derivative of head with respect to time; and $\Delta x_i\, \Delta y_j\, \Delta z_k$ is the volume of cell (i, j, k). The time derivative of head is expressed in terms of specific heads and time by defining the head difference as $\Delta h = h^m_{i,j,k} - h^{m-1}_{i,j,k}$ and the time interval as $\Delta t = t_m - t_{m-1}$:

$$\frac{\Delta h}{\Delta t} = \frac{h^m_{i,j,k} - h^{m-1}_{i,j,k}}{t_m - t_{m-1}} \tag{9.5.18}$$

The rate at which water is stored in or released from cell (i, j, k) is expressed as

$$\frac{\Delta V}{\Delta t} = \mathrm{SS}_{i,j,k}\left(\Delta x_i \Delta y_j \Delta z_k\right) \frac{h^m_{i,j,k} - h^{m-1}_{i,j,k}}{t_m - t_{m-1}} \tag{9.5.19}$$

External flows (sources and stresses) from outside the aquifer into each cell, such as recharge, streams, and flow out of each cell—such as evapotranspiration and well pumpage for each individual cell—must also be taken into account. The total external flow for cell (i, j, k) is designated $W_{i,j,k}$, which is the combination of source and/or stress terms for an individual cell expressed as

$$W_{i,j,k} = \sum_{n=1}^{N} p_{i,j,k,n} h_{i,j,k} + \sum_{n=1}^{N} q_{i,j,k,n} = P_{i,j,k} h_{i,j,k} + Q_{i,j,k} \tag{9.5.20}$$

where N is the number of external sources or stresses affecting cell (i, j, k), and $p_{i,j,k,n}$ and $q_{i,j,k,n}$ are constants that describe the individual external sources or stresses. These constants for the MODFLOW model are described in more detail in subsection 9.6.3.

The continuity equation for cell (i, j, k) is expressed as

$$\begin{aligned} &q_{i,j-1/2,k} + q_{i,j+1/2,k} + q_{i-1/2,j,k} + q_{i+1/2,j,k} + q_{i,j,k-1/2} \\ &\quad + q_{i,j,k+1/2} + W_{i,j,k} = \mathrm{SS}_{i,j,k} \frac{\Delta h_{i,j,k}}{\Delta t} \left(\Delta x_i \Delta y_j \Delta z_k\right) \end{aligned} \tag{9.5.21}$$

Equations 9.5.11–9.5.16, 9.5.19, and 9.5.20 are substituted into 9.5.21, resulting in the following finite difference approximation for cell (i, j, k):

$$\begin{aligned} &CY_{i,j-1/2,k}(h_{i,j-1,k} - h_{i,j,k}) + CY_{i,j+1/2,k}(h_{i,j+1,k} - h_{i,j,k}) + CX_{i-1/2,j,k}(h_{i-1,j,k} - h_{i,j,k}) \\ &\quad + CX_{i+1/2,j,k}(h_{i+1,j,k} - h_{i,j,k}) + CZ_{i,j,k-1/2}(h_{i,j,k-1} - h_{i,j,k}) + CZ_{i,j,k+1/2}(h_{i,j,k+1} - h_{i,j,k}) \\ &\quad + P_{i,j,k} h_{i,j,k} + Q_{i,j,k} = SS_{i,j,k}(\Delta x_i \Delta y_j \Delta z_k)(\Delta h_{i,j,k}/\Delta t) \end{aligned} \tag{9.5.22}$$

The flow terms can be expressed in terms of h^m at time t_m as

$$\begin{aligned} &CY_{i,j-1/2,k}\left(h^m_{i,j-1,k} - h^m_{i,j,k}\right) + CY_{i,j+1/2,k}\left(h^m_{i,j+1,k} - h^m_{i,j,k}\right) + CX_{i-1/2,j,k}\left(h^m_{i-1,j,k} - h^m_{i,j,k}\right) \\ &\quad + CX_{i+1/2,j,k}\left(h^m_{i+1,j,k} - h^m_{i,j,k}\right) + CZ_{i,j,k-1/2}\left(h^m_{i,j,k-1} - h^m_{i,j,k}\right) + CZ_{i,j,k+1/2}\left(h^m_{i,j,k+1} - h^m_{i,j,k}\right) \\ &\quad + P_{i,j,k} h^m_{i,j,k} + Q_{i,j,k} = \mathrm{SS}_{i,j,k}\left(\Delta x_i \Delta y_j \Delta z_k\right) \frac{\left(h^m_{i,j,k} - h^{m-1}_{i,j,k}\right)}{t_m - t_{m-1}} \end{aligned} \tag{9.5.23}$$

This equation can be rearranged so that all terms of h^m containing heads at the current time step are grouped on the left-hand side of the equation and all remaining known terms independent of heads at the current time step are on the right-hand side. The resulting equation is

$$\begin{aligned} &CZ_{i,j,k-1/2}\left(h^m_{i,j,k-1}\right) + CX_{i-1/2,j,k}\left(h^m_{i-1,j,k}\right) + CY_{i,j-1/2,k}\left(h^m_{i,j-1,k}\right) \\ &+\left(-CZ_{i,j,k-1/2} - CX_{i-1/2,j,k} - CY_{i,j-1/2,k} - CY_{i,j+1/2,k}\right. \\ &\quad \left. -CZ_{i}+_{1/2,j,k} - CZ_{i,j,k+1/2} + HCOF_{i,j,k}\right) h^m_{i,j-1,k} \\ &+CY_{i,j+1/2,k}\left(h^m_{i,j+1,k}\right) + CX_{i+1/2,j,k}\left(h^m_{i+1,j,k}\right) + CZ_{i,j,k+1/2}\left(h^m_{i,j,k+1}\right) = RHS_{i,j,k} \end{aligned} \tag{9.5.24}$$

where

$$HCOF_{i,j,k} = P_{i,j,k} - \frac{SC1_{i,j,k}}{(t_m - t_{m-1})} \qquad \left[L^2/T\right]$$

$$RHS_{i,j,k} = -Q_{i,j,k} - \frac{SC1_{i,j,k} h^{m-1}_{i,j,k}}{(t_m - t_{m-1})} \qquad \left[L^3/T\right]$$

and

$$SC1_{i,j,k} = SS_{i,j,k}\left(\Delta x_i \Delta y_j \Delta z_k\right) \qquad \left[\mathrm{L}^2\right]$$

Expressing Equation 9.6.24 for each variable-head cell in the aquifer results in a system of equations of the following matrix form:

$$[A]\{h\}=\{q\} \tag{9.5.25}$$

where $[A]$ is a matrix of the coefficients of heads from the left side of Equation 9.5.24 for all active nodes in the mesh; $\{h\}$ is the vector of unknown heads at the end of time step m for all nodes in the mesh; and $\{q\}$ is the vector of constant terms, the right side of Equation 9.5.24, for all nodes of the mesh.

9.5.2 Simulation of Boundaries

In order to simulate boundary conditions, cells are grouped as constant-head cells and inactive (or no-flow) cells. *Constant-head cells* have a specified value through all time steps of the simulation. *Inactive cells* do not allow flow into or out of the cell. The remaining cells of a finite difference grid system (mesh) are variable head cells. The finite difference Equation 9.5.24 is formulated for each variable-head cell in the mesh. The system of finite difference equations is solved simultaneously for each time step in the simulation.

The constant-head and no-flow cells are used to represent conditions of various hydrologic conditions, as illustrated in Fig. 9.5.5. Even though the aquifer is irregular in shape the mesh defining the aquifer is always rectangular in outline. No-flow cells are used to delete the portion of the array of cell beyond the aquifer boundary. Figure 9.5.5 shows constant-head cells along one section of the boundary to simulate direct contact with a major surface water body. Boundary conditions, such as areas of constant flow or areas where inflow varies with head, can be simulated as an external source or through a combination of external source and a no-flow cell.

9.5.3 Vertical Discretization

The range of vertical discretization of an aquifer cross section (see Fig. 9.5.6) can be visualized simply as an extension of areal discretization in an effort to represent individual aquifers or

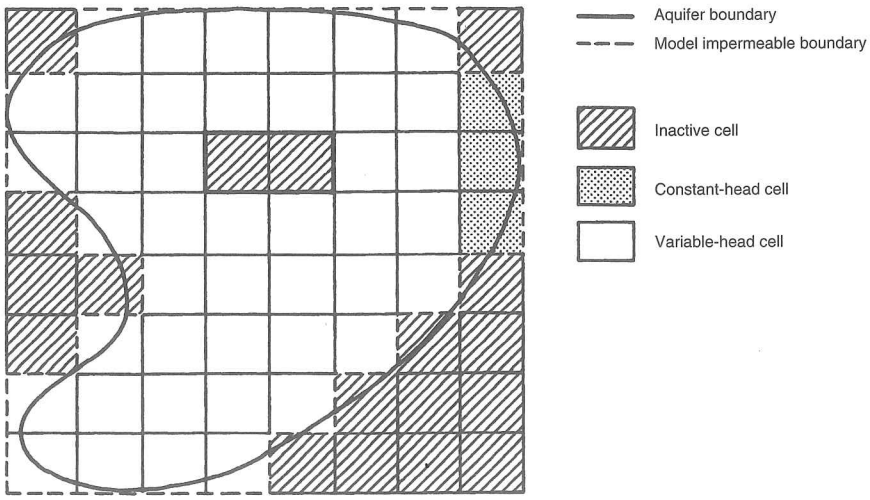

Figure 9.5.5. Discretized aquifer showing boundaries and cell designations (McDonald and Harbaugh[39]).

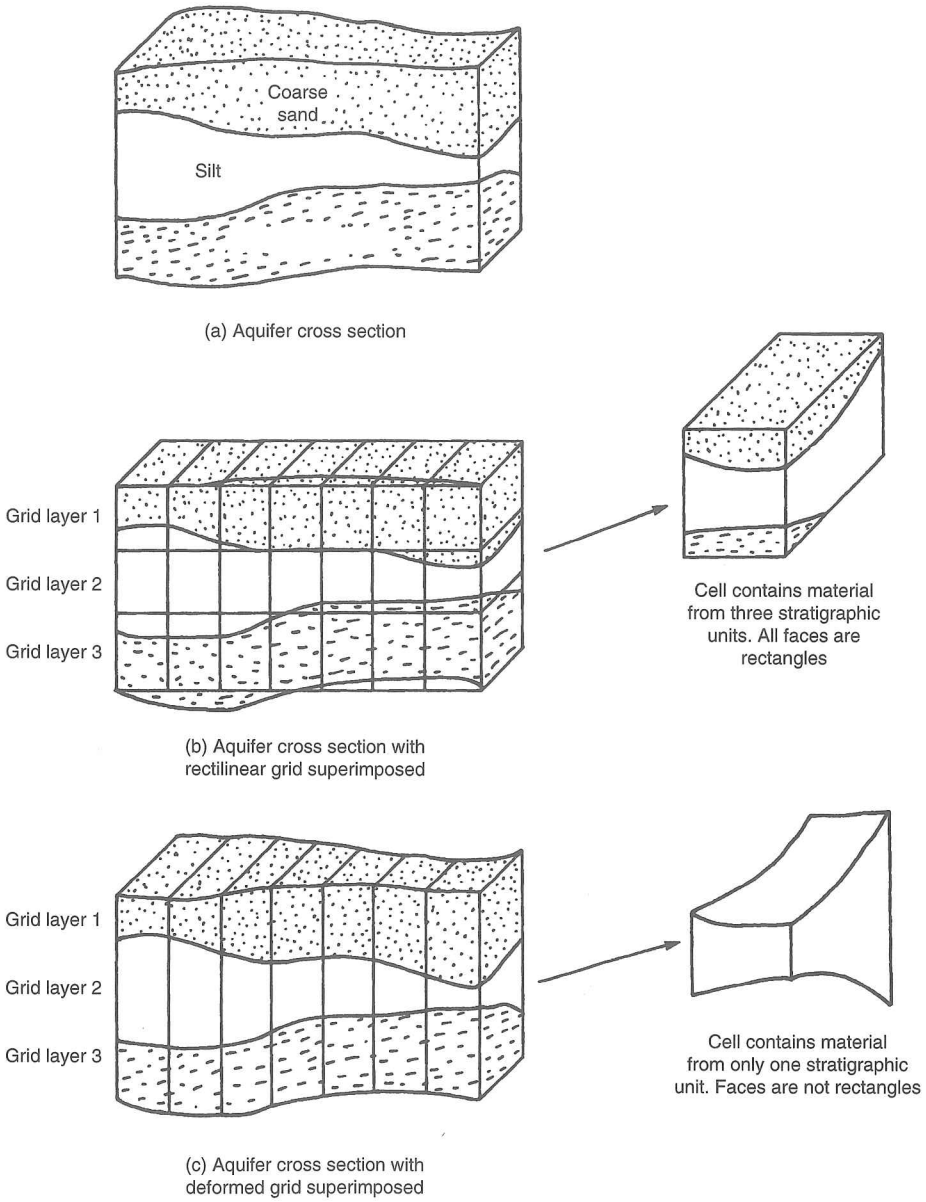

Figure 9.5.6. Schemes of vertical discretization.[39]

permeable zones by individual layers of the model. The simpler approach (Figure 9.5.6*b*) leads to a rigid superposition of an orthogonal three-dimensional mesh on the geohydrologic system. In the second approach (Figure 9.5.6*c*), the model layer thickness is considered variable in order to simulate the varying thickness of the geohydrologic units leading to a deformed mesh.

The advantage of the second approach is that the uniform hydraulic properties of a cell are better approximated when the model layers conform to the geohydrologic units. Also, greater accuracy is expected if model layers correspond to intervals within which vertical headloss is negligible, which is more likely using the approach shown in Figure 9.5.6*c*. However, the deformed mesh of Figure 9.5.6*c* fails to conform to the assumptions of the model equations. As an example, cells may no longer have rectangular sides and the major axes of hydraulic conductivity may not be aligned with the model axis, both introducing errors.

In practice, vertical discretization schemes turn out to be a combination of the viewpoints illustrated in Figure 9.5.6 (McDonald and Harbaugh[39]). Figure 9.5.7 illustrates a system consisting of two sand layers separated by a clay layer. Each of the units is of equal thickness so that each of the units could be represented by a single layer without deformation of the mesh; however, the flow pattern is much more complicated as illustrated by the flow lines. In this case, several layers must be used to represent each layer. Figure 9.5.8 illustrates another case of a sand and clay system in which pumpage from the sands is sustained partially by vertical flow of water released from storage in the clay. Several model layers would be required to determine the pattern of storage release in the clay as shown in the figure. In the case that the storage is released only in the sands, the flow would be nearly horizontal with the flow in the clay nearly vertical. A single layer could be used for each sand unit and the clay layer could be represented by a vertical conductance between sand layers, which is sometimes referred to as a quasi–three-dimensional approach. Each of these vertical-discretization approaches leads to a set of model equations of the form of Equation 9.5.24.

9.5.4 Hydraulic Conductance Equations

Conductance has previously been defined as the product of hydraulic conductivity and cross-sectional area of flow divided by the length of the flow path. Start with Darcy's law defining

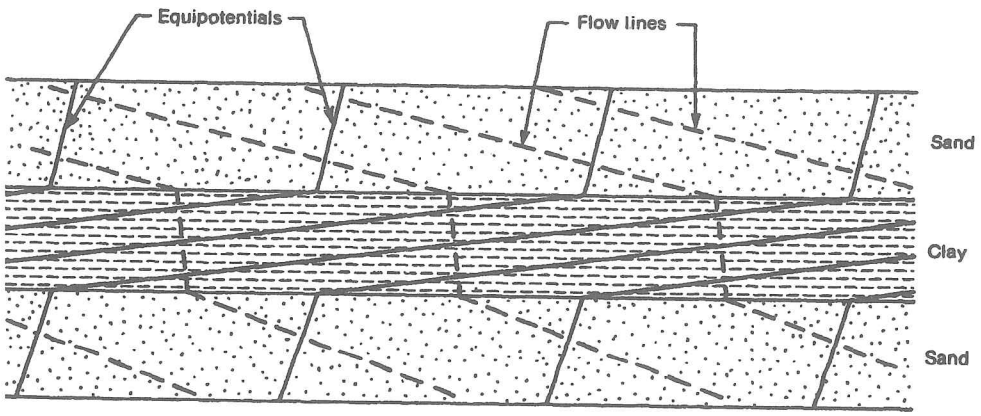

Figure 9.5.7. Possible pattern of flow in a cross section consisting of two high conductivity units separated by a low conductivity unit.[39]

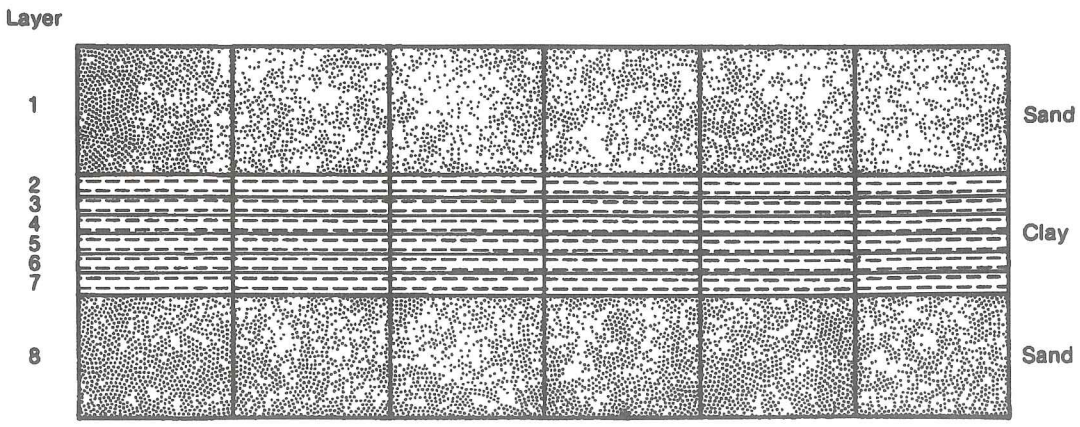

Figure 9.5.8. A cross section in which a low conductivity unit is represented by six model layers.[39]

one-dimensional flow in a prism of porous medium (Figure 3.1.1) as $Q = -KA(h_2 - h_1)/L$; where Q is the volumetric flow, K is the hydraulic conductivity, A is the cross-sectional area perpendicular to flow, $h_1 - h_2$ is the head difference across the prism parallel to flow, and L is the length of the prism parallel to the flow path. Then the hydraulic conductance is defined as $C = KA/L$ and Darcy's law can be written as $Q = C(h_1 - h_2)$. Another form of the hydraulic conductance for horizontal flow in a prism is $C = TB/L$ where T is the transmissivity in the direction of flow L^2/T and B is the width of the prism.

Hydraulic conductance is defined for a particular prism of material and for a particular direction of flow. Anisotropic media are characterized by three principal directions of hydraulic conductivity so that the hydraulic conductances of a prism differ in the three directions.

Now consider a prism of porous medium consisting of two or more subprisms in a series, as shown in Figure 9.5.9. Knowing the conductance in each subprism, we can compute a hydraulic conductance representing the entire prism, referred to as the *equivalent hydraulic conductance*. The equivalent hydraulic conductance for the entire prism is $C = Q/(h_A - h_B)$. The total head loss (referring to Figure 9.5.9) is

$$\sum_{i=1}^{n} \Delta h_i = h_A - h_B \tag{9.5.26}$$

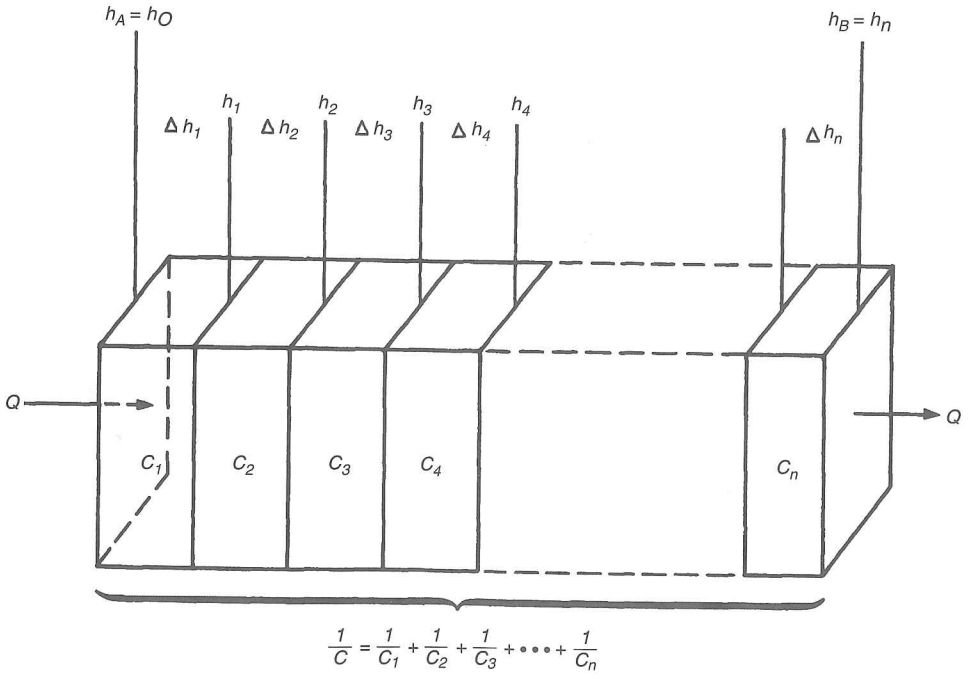

Figure 9.5.9. Calculation of conductance through several prisms in a series.[39]

And substituting for head change across each section using Darcy's law then leads to

$$\sum_{i=1}^{n} \frac{q_i}{C_i} = h_A - h_B \tag{9.5.27}$$

Because flow is one dimensional and it is assumed that there is no accumulation or depletion in storage; then all q_i are equal to the total flow Q. Then

$$Q\sum_{i=1}^{n} \frac{1}{C_i} = h_A - h_B \quad \text{and} \quad \frac{h_A - h_B}{Q} = \sum_{i=1}^{n} \frac{1}{C_i} \tag{9.5.28}$$

From $C = Q/(h_A - h_B)$ and Equation 9.5.28, the equivalent hydraulic conductance is

$$\frac{1}{C} = \sum_{i=1}^{n} \frac{1}{C_i} \tag{9.5.29}$$

which states that for a set of hydraulic conductances arranged in series, the inverse of the equivalent conductance equals the sum of the inverses of the individual conductances. For two sections, the equivalent hydraulic conductance is $C = C_1C_2/(C_1 + C_2)$ which explains the form of Equation 9.5.3.

9.6 MODFLOW-2000 DESCRIPTION

9.6.1 Model Introduction

MODFLOW-2000 is a computer program that simulates one-, two-, or three-dimensional groundwater flow using a finite difference solution of the model formulation presented in Section 9.5 of this chapter, MODFLOW, the original computer program, was first published by McDonald and Harbaugh.[38] This program was developed using a modular structure for ease in adapting the code for particular applications. The second version of MODFLOW, documented in McDonald and Harbaugh,[39] was referred to as MODFLOW-88. The third version was documented by Harbaugh and McDonald[21, 22] and was referred to as MODFLOW-96. The most recent version, MODFLOW-2000, documented in Harbaugh et al.,[20] includes many capabilities added since the original computer program. This section briefly describes these capabilities.

MODFLOW-2000 can simulate steady and nonsteady flow in an irregularly shaped flow system in which aquifer layers can be confined, unconfined, or a combination of confined and unconfined. Flow from external stresses, such as flow to wells, areal recharge, evapotranspiration, flow to drains, and flow through river beds, can be simulated. The hydraulic conductivities or transmissivities for any layer may differ spatially and be anisotropic (restricted to having the principal directions aligned with the grid axes), and the storage coefficient may be heterogeneous. Specified head and specified flux boundaries can be simulated, as can a head-dependent flux across the model's outer boundary, which allows water to be supplied by a boundary block in the modeled area at a rate proportional to the current head difference between a source of water outside the modeled area and the boundary block. MODFLOW-2000 has been expanded to simulate solute transport and parameter estimation.

The MODFLOW-2000 computer program is divided into a main program and a series of independent subroutines called modules. The modules are grouped into packages that deal with a single aspect of the simulation. The packages are listed and briefly described in Table 9.6.1. Individual packages may or may not be required, depending on the problem being

Table 9.6.1 Processes, Packages, and Additional Capabilities of MODFLOW-2000 (Version 1.1, 1/17/2001)

Processes	Packages	Additional Capabilities
GWF1—Ground-Water Flow Process	BAS6—Basic Package	HYDMOD—Hydrograph Option[17]
SEB1—Sensitivity Process	BCF6—Block-Centered Flow Package[15, 21, 22, 40]	
OBS1—Observation Process	LPF1—Layer-Property Flow Package	
PES1—Parameter-Estimation Process	RIV6—River Package	
	DRN6—Drain Package	
	WEL6—Well Package	
	GHB6—General Head Boundary Package	
	RCH6—Recharge Package	
	EVT6—Evapotransipiration Package	
	CHD6—Time-Variant Specified-Head Package[36]	
	HFB6—Horizontal Flow Barrier Package[28]	
	SIP5—Strongly Implicit Procedure Package	
	SOR5—Slice Successive Over-Relaxation Package	
	PCG2—Version 2 of Preconditioned Conjugate Gradient Package[24]	
	DE45—Direct Solver[19]	
	STR6—Streamflow-Routing Package[53]	
	ADV2—Advective-Transport Observation Package[2]	
	RES1—Reservoir Package[10]	
	FHB1—Flow and Head Boundary Package[35]	
	IBS6—Interbed Storage (Subsidence) Package[36]	
	HUF1—Hydrogeologic-Unit Flow Package[3]	
	LAK3—Lake Package[41]	
	ETS1—Evapotranspiration with a Segmented Function Package[6]	
	DRT1—Drains with Return Flow Package[6]	

solved. The basic documentation for MODFLOW is contained in Harbaugh and McDonald,[21, 22] Harbaugh et al.,[20] Hill et al.,[26] and McDonald and Harbaugh.[39]

9.6.2 Space and Time Discretization

The physical size of the finite difference grid is provided through input to the program. In all versions of MODFLOW, the finite difference grid is assumed to be rectangular horizontally and can be distorted vertically as illustrated in Figure 9.6.1. The horizontal grid dimensions are specified by the cell widths DELR and DELC (Figure 9.6.1a). Columns are numbered starting from the left side of the grid and rows are numbered starting from the upper edge (plan view) of the grid. All cells in a column have the same width and all cells in a row have the same width. Layers are numbered starting from the top layer down (see Figure 9.6.1b). The elevation of the top of Layer 1 and the bottom elevation of each layer for each cell are used to determine the thickness of each cell. A confining bed through which only vertical flow exists can be simulated below each layer except the bottom layer. This simulation of confining beds is referred to as the quasi–three-dimensional (quasi-3D) approach.[39]

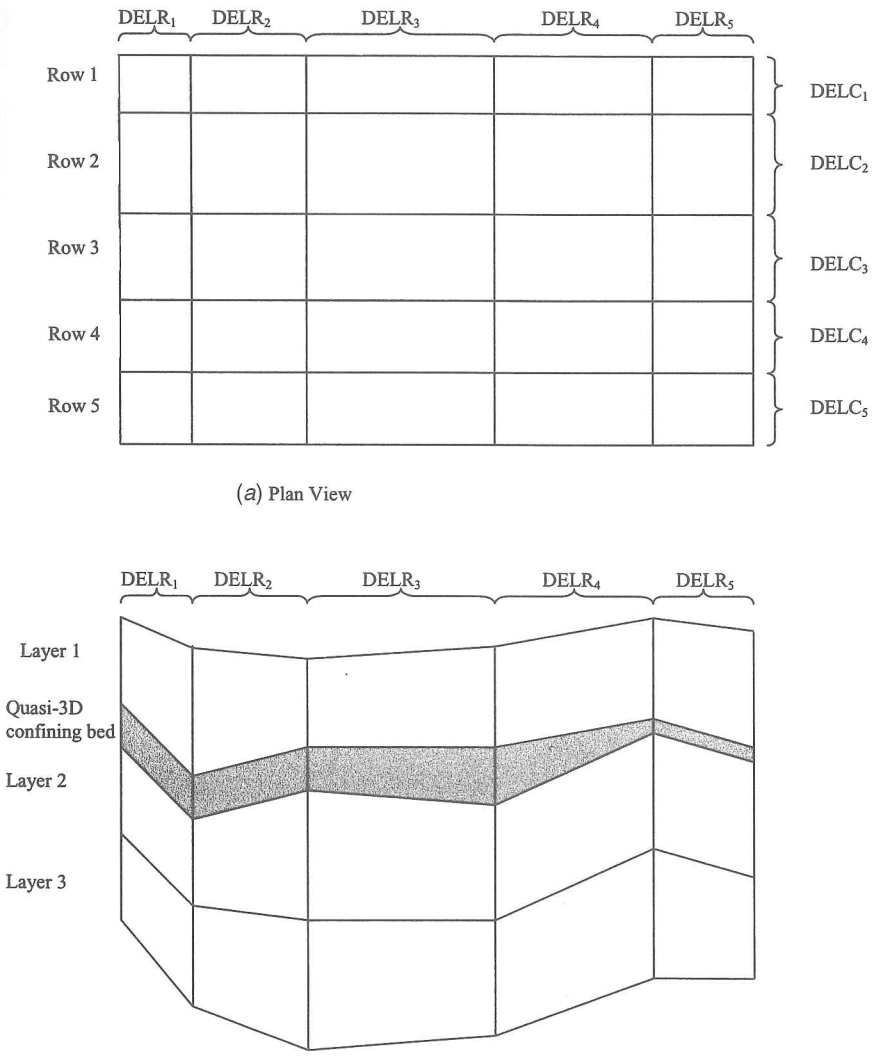

Figure 9.6.1. Finite difference grid with (*a*) plan view and (*b*) cross-sectional view (Harbaugh et al.[20]).

Time discretization is dealt with through time steps, which are grouped into stress periods. For each stress period, the user specifies the total length (PERLEN), the number of time steps (NSTP), and the multiplier for the length of the time step $n-1$ times TSMULT. This procedure develops a geometric series with the length of the first time step given as

$$\Delta t_1 = \text{PERLEN}\left(\frac{\text{TSMULT}-1}{\text{TSMULT}^{\text{NSTP}}-1}\right) \tag{9.6.1}$$

9.6.3 External Sources and Stresses

9.6.3.1 Rivers and Streams

The effects of flow between surface water features and groundwater systems are modeled by adding terms for the seepage to or from the surface water feature to the finite difference model

Equation 9.5.24. Flow between a stream and the groundwater system, $W_{i,j,k}$ = QRIV, is expressed as

$$\begin{aligned} \text{QRIV} &= \text{CRIV}(\text{HRIV} - h_{i,j,k}), \quad h_{i,j,k} > \text{RBOT} \\ \text{QRIV} &= \text{CRIV}(\text{HRIV} - \text{RBOT}), \quad h_{i,j,k} \leq \text{RBOT} \end{aligned} \tag{9.6.2}$$

where CRIV is the hydraulic conductance defined as KLB/M, in which K is the hydraulic conductance of the streambed layer, L is the length of the stream reach contained within the cell, B is the width of the stream reach, and M is the thickness of the streambed material; HRIV is the head in the stream; $h_{i,j,k}$ is the head at the node in the cell underlying the stream reach; and RBOT is the elevation of the bottom of the streambed layer.

9.6.3.2 Areal Recharge

Areal recharge, which most commonly occurs as a result of precipitation percolating into the groundwater system, $W_{i,j,k} = \text{QR}_{i,j}$, is expressed as

$$\text{QR}_{i,j} = I_{i,j} \times \text{DELR}_j \times DELC_i \tag{9.6.3}$$

where $\text{QR}_{i,j}$ is the recharge flow rate applied to horizontal cell (i, j), expressed as water volume per unit time, and $I_{i,j}$ is the recharge flux (length per unit time) applicable to the area $\text{DELR}_j\text{DELC}_i$.

9.6.3.3 Drains

Buried and open drains are shown in Figure 9.6.2. The flow into a drain is illustrated in the cross-section through cell (i, j, k) in Figure 9.6.3. Flow in the drain is assumed to be only partially full, so the head within the drain is approximately equal to the median drain elevation, $d_{i,j,k}$. The head, $h_{i,j,k}$, is the average head for the cell. There are three processes of flow into the drain: convergent flow through the drain, flow through immediately around the drain with a different hydraulic conductivity, and flow through the wall of the drain. Each of these processes creates head losses that are assumed to be proportional to the discharge, $\text{QD}_{i,j,k}$, with the total head loss $h_{i,j,k} - d_{i,j,k}$. The drain function, $W_{i,j,k} = \text{QD}_{i,j,k}$, is expressed as

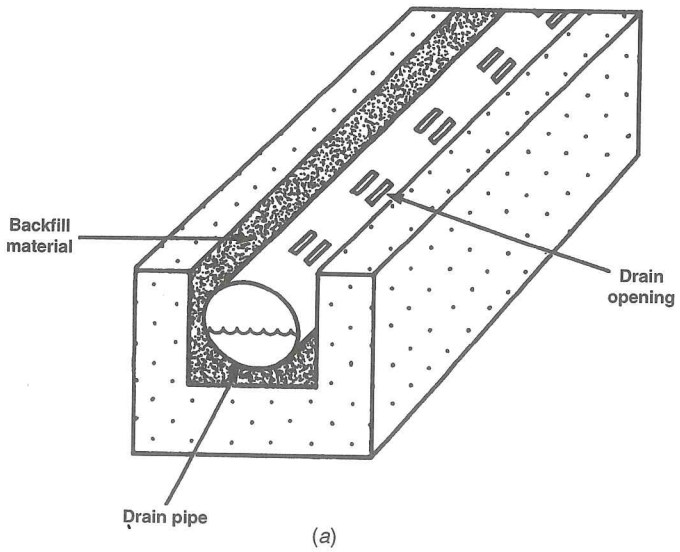

Figure 9.6.2. Factors affecting head loss immediately around a drain: (*a*) buried drain pipe in backfilled ditch and (*b*) open drain (McDonald and Harbaugh[39]).

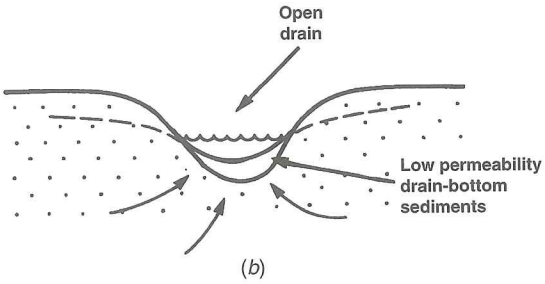

Figure 9.6.2 (continued). Factors affecting head loss immediately around a drain: (*a*) buried drain pipe in backfilled ditch and (*b*) open drain (McDonald and Harbaugh[39]).

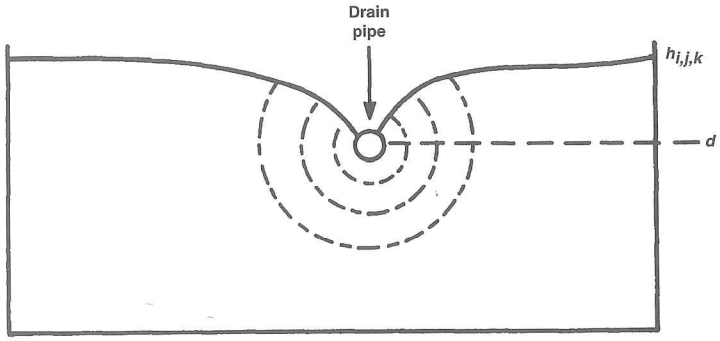

Figure 9.6.3. Cross section through cell (*i, j, k*) illustrating head loss in convergent flow into drain. (McDonald and Harbaugh[39]).

$$QD_{i,j,k} = CD_{i,j,k}\,(h_{i,j,k} - d_{i,j,k}) \qquad \text{for } h_{i,j,k} > d_{i,j,k} \tag{9.6.4}$$

$$QD_{i,j,k} = 0 \qquad \text{for } h_{i,j,k} \le d_{i,j,k} \tag{9.6.5}$$

where $CD_{i,j,k}$ is a lumped or equivalent conductance describing all of the head loss between the drain and the cell (see McDonald and Harbaugh[39]). See Banta[6] for more information on modeling drains with return flows.

9.6.3.4 Evapotranspiration

To simulate the effects of plant transpiration and direct evaporation of water from the saturated groundwater, the volumetric rate of flow from a given cell is required. The volumetric rate of evaporation, $W_{i,j,k} = Q_{ETi,j,k}$, is the product of the loss rate per unit area of the cell and the horizontal surface area, $DELR_j\ DELC_i$, given as

$$Q_{ETi,j} = R_{ETi,j} \times DELR_j \times DELC_i \tag{9.6.6}$$

where $R_{ETi,j}$ is the rate of loss per unit surface area of water table due to evapotranspiration, given as

$$\begin{aligned} R_{ETi,j} &= R_{ETMi,j} && h_{i,j,k} > h_{si,j} \\ R_{ETi,j} &= 0 && h_{i,j,k} < h_{si,j} - d_{i,j} \\ R_{ETi,j} &= R_{ETMi,j}\left[\frac{h_{i,j,k} - (h_{si,j} - d_{i,j})}{d_{i,j}}\right] && (h_{si,j} - d_{i,j}) \le h_{i,j,k} \le h_{si,j} \end{aligned} \tag{9.6.7}$$

in which $h_{si,j}$ is the water table elevation at which the maximum value of evapotranspiration loss occurs, $R_{ETMi,j}$ is the maximum possible value of $R_{ETi,j}$, and $d_{i,j}$ is the cutoff or extinction depth so that when the distance between $h_{si,j}$ and $h_{i,j,k}$ exceeds $d_{i,j}$, then evapotranspiration ceases. See Banta[6] for modeling evapotranspiration with a segmented function.

9.6.3.5 General Head Boundary

The flow $Q_{bi,j,k}$ into or out of a cell from an external source with a known head is proportional to the difference between the head in cell, $h_{i,j,k}$, and the head assigned to the external source, $h_{bi,j,k}$, as

$$Q_{bi,j,k} = C_{bi,j,k}\,(h_{bi,j,k} - h_{i,j,k}) \tag{9.6.8}$$

where $C_{bi,j,k}$ is the conductance between the external source and cell (i, j, k).

9.6.3.6 Wells

For injection wells, the source strength is

$$W_{i,j,k} = \mathrm{QW}_{i,j,k}\,(t_m) \tag{9.6.9}$$

where $\mathrm{QW}_{i,j,k}(t_m)$ is the well injection discharge during the stress period at time t_m.

9.6.4 Hydraulic Conductance—Layer-Property Flow Package (LPF)

9.6.4.1 Horizontal Hydraulic Conductance

MODFLOW solves the finite difference Equations 9.5.24 using equivalent hydraulic conductances between nodes of adjacent cells, as explained in Section 9.5.4. CR (along rows) and CC (along columns) are the horizontal equivalent hydraulic conductance terms between adjacent horizontal nodes. The LPF Package in MODFLOW-2000 reads data defining the horizontal hydraulic conductivity for individual cells and uses this information to compute the equivalent hydraulic conductance between nodes, using one of three methods.

The first method assumes a constant transmissivity (hydraulic conductivity times thickness) within a cell, but allows a discrete change in transmissivity at the boundary between the cells. Because it is at the center of the cells, the hydraulic conductance between nodes is the equivalent hydraulic conductance of two half cells in series, as shown in Figure 9.6.4. Using $C = C_1C_2/(C_1 + C_2)$, we obtain the conductance CR given in Figure 9.6.4 and the conductance CC as

$$\mathrm{CR}_{i,j+\frac{1}{2},k} = \frac{\left[\dfrac{\mathrm{TR}_{i,j,k}\mathrm{DELC}_i}{(1/2)\mathrm{DELR}_j}\right]\left[\dfrac{\mathrm{TR}_{i,j+1,k}\mathrm{DELC}_i}{(1/2)\mathrm{DELR}_{j+1}}\right]}{\dfrac{\mathrm{TR}_{i,j,k}\mathrm{DELC}_i}{(1/2)\mathrm{DELR}_j} + \dfrac{\mathrm{TR}_{i,j+1,k}\mathrm{DELC}_i}{(1/2)\mathrm{DELR}_{j+1}}} \tag{9.6.10}$$

where $\mathrm{TR}_{i,j,k}$ is the transmissivity in the row direction at cell (i, j, k). This approach for calculating interblock conductance is the *harmonic mean method.* $\mathrm{CC}_{i+1/2,k}$ is computed in the same manner. The equations for CR and CC are used unless the transmissivities of both cells are zero, resulting in an equivalent hydraulic conductance of zero.

Goode and Appel[15] describe three alternative approaches for calculating horizontal hydraulic conductances. One method assumes that the transmissivity varies linearly between nodes, referred to as the *logarithmic-mean interblock transmissivity method.* The second method assumes a flat, homogeneous aquifer with a water table defining the *arithmetic-mean interblock transmissivity method.* The third method assumes a flat aquifer with a water table in which hydraulic conductivity varies linearly between nodes defining the *arithmetic-mean thickness and logarithmic-mean hydraulic conductivity method.* The first and third methods are also included in the LPF package in MODFLOW-2000. Harbaugh[18] describes a generalized

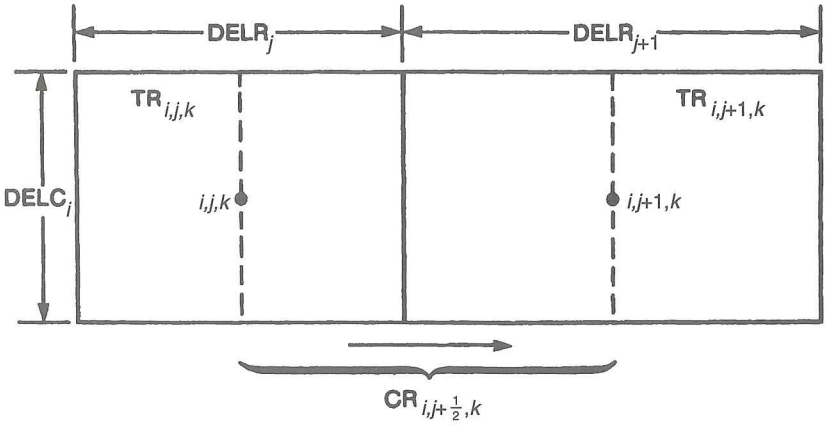

$$\frac{1}{CR_{i,j,+\frac{1}{2},k}} = \frac{1}{\left(\frac{TR_{i,j,k}DELC_i}{\left(\frac{DELR_j}{2}\right)}\right)} + \frac{1}{\left(\frac{TR_{i,j,+l,k}DELC_i}{\left(\frac{DELR_{j+1}}{2}\right)}\right)}$$

$$CR_{i,j+\frac{1}{2},k} = 2\,DELC \times \frac{TR_{i,j,k}TR_{i,j+1,k}}{TR_{i,j,k}DELR_{j+1} + TR_{i,j+1,k}DELR_j}$$

$TR_{i,j,k}$ Is transmissivity in the row direction in cell (i,j,k)

$CR_{i,j+\frac{1}{2},k}$ Is conductance in the row direction between nodes (i,j,k) and $(i,j+1,k)$

Figure 9.6.4. Calculation of conductance between nodes using transmissivity and dimensions of cells (McDonald and Harbaugh[39]).

finite-difference interblock transmissivity for unconfined aquifers and for aquifers having smoothly varying transmissivity.

9.6.4.2 Vertical Hydraulic Conductance

The vertical hydraulic conductance is calculated assuming that nodes are in the center of cells and discrete changes in vertical hydraulic conductivity occur at the boundaries of the layers, as illustrated in Figure 9.6.5. Using Equation 9.5.29 with the hydraulic conductance for each half cell results in

$$\frac{1}{CV_{i,j,k+\frac{1}{2}}} = \frac{1}{\frac{DELR_j DELC_i VK_{i,j,k}}{\left(\frac{1}{2}\right)THICK_{i,j,k}}} + \frac{1}{\frac{DELR_j DELC_i VK_{i,j,k+1}}{\left(\frac{1}{2}\right)THICK_{i,j,k+1}}} \tag{9.6.11}$$

where $VK_{i,j,k}$ is the vertical hydraulic conductivity of cell (i,j,k) and $THICK_{i,j,k}$ is the saturated thickness of cell (i, j, k). Simplifying Equation 9.6.11 results in

$$\frac{1}{CV_{i,j,k+\frac{1}{2}}} = \frac{DELR_j DELC_i}{\frac{\left(\frac{1}{2}\right)THICK_{i,j,k}}{VK_{i,j,k}} + \frac{\left(\frac{1}{2}\right)THICK_{i,j,k+1}}{VK_{i,j,k+1}}} \tag{9.6.12}$$

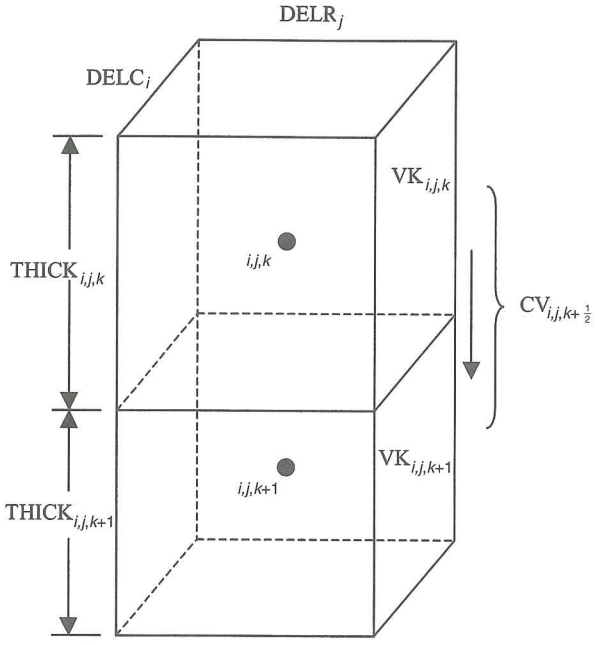

Figure 9.6.5. Calculation of vertical conductance between two nodes (Harbaugh et. al.[20]).

The calculation of vertical conductance between two nodes with a semiconfining unit in between (Figure 9.6.6) assumes that the semiconfining layer makes no measurable contribution to the horizontal conductance or the storage capacity of either model layer. Under such assumptions, the confining bed restricts vertical flow between the cells. A quasi–three-dimensional approach (McDonald and Harbaugh[39]) is used. In this approach, three intervals (lower half of upper aquifer, semiconfining unit, and the upper half of the lower aquifer) are represented in the summation of conductance between the nodes. Using Equation 9.5.29, we obtain for the vertical hydraulic conductance

$$\frac{1}{CV_{i,j,k+\frac{1}{2}}} = \frac{1}{\dfrac{\text{DELR}_j\text{DELC}_i\text{VK}_{i,j,k}}{\left(\frac{1}{2}\right)\text{THICK}_{i,j,k}}} + \frac{1}{\dfrac{\text{DELR}_j\text{DELC}_i\text{VKCB}_{i,j,k}}{\text{THICK}_{CB}}} + \frac{1}{\dfrac{\text{DELR}_j\text{DELC}_i\text{VK}_{i,j,k+1}}{\left(\frac{1}{2}\right)\text{THICK}_{i,j,k+1}}} \tag{9.6.13}$$

where $\text{VKCB}_{i,j,k}$ is the hydraulic conductivity of the semiconfining unit between cells (i, j, k) and $(i, j, k + 1)$ and THICK_{CB} is the thickness of the semiconfining unit. Equation 9.6.13 can be simplified to

$$CV = \frac{\text{DELR}_j\ \text{DELC}_i}{\dfrac{\left(\frac{1}{2}\right)\text{THICK}_{i,j,k}}{\text{VK}_{i,j,k}} + \dfrac{\text{THICK}_{CB}}{\text{VKCB}_{i,j,k}} + \dfrac{\left(\frac{1}{2}\right)\text{THICK}_{i,j,k+1}}{\text{VK}_{i,j,k+1}}} \tag{9.6.14}$$

9.6.4.3 Vertical Flow Calculation under Dewatered Conditions

A modification to the vertical flow calculation is required when a cell in a convertible layer is unconfined and the cell immediately above is fully or partially saturated (see Figure 9.6.7). This modification (vertical flow correction) is applied to every iteration of the solution process.

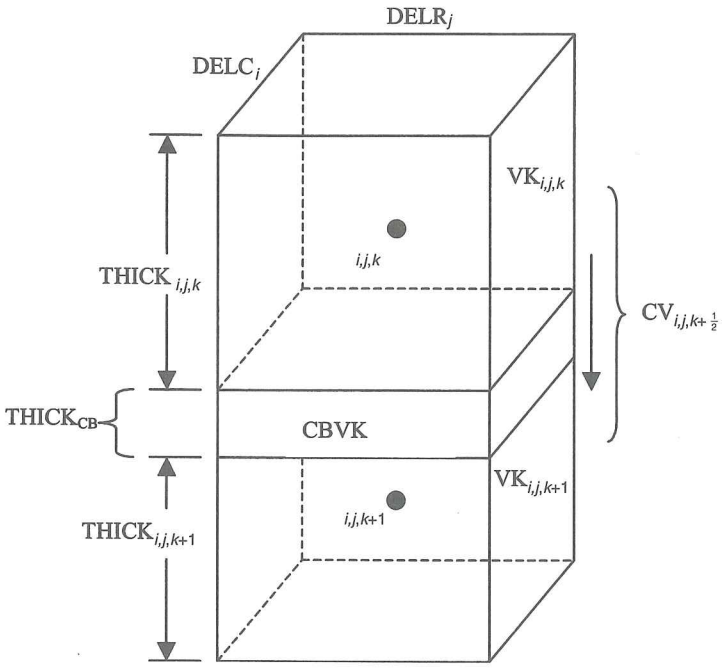

Figure 9.6.6. Calculation of vertical conductance between two nodes with a semi-confining unit between.[20]

The actual flow between the nodes in the upper and lower cells is the flow through the confining bed, $q_{i,j,k+1/2}$ computed using

$$q_{i,j,k+\frac{1}{2}} = \mathrm{CV}_{i,j,k+\frac{1}{2}}\left(\mathrm{TOP}_{i,j,k+1} - h_{i,j,k}\right) \tag{9.6.15}$$

so that the flow is downward from cell (i, j, k) to cell $(i, j, k + 1)$ but is not dependent on $h_{i,j,k+1}$. Equation 9.6.15 could be substituted into the finite difference Equation 9.4.24; however, the

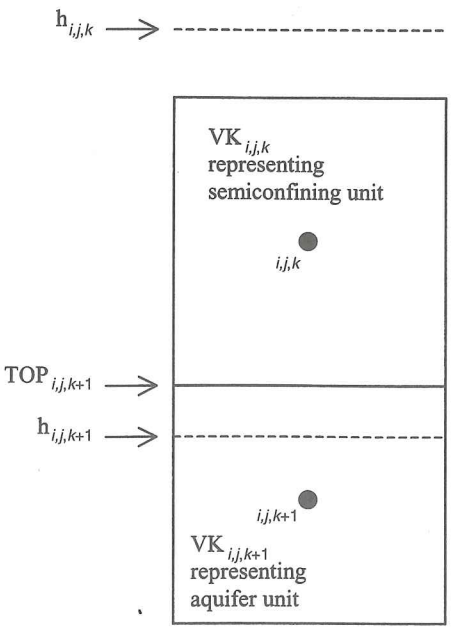

Figure 9.6.7. Situation in which a correction is required to limit the downward flow into cell $(i, j, k + 1)$, as a result of partial desaturation of the cell.[20]

matrix A in Equation 9.4.25 would be asymmetric, generating problems in the solution process. Alternatively, in MOFLOW-2000, the flow is computed as $q_{i,j,k+1/2} = \mathrm{CV}_{i,j,k+1/2}(h_{i,j,k+1}, -\mathrm{h}_{i,j,k})$ so that this term remains on the left side of Equation 9.4.24. Then a correction term q_c is added to the right side to compensate for allowing the computed flow to remain on the left side of Equation 9.4.24,

$$q_c^n = \mathrm{CV}_{i,j,k+\frac{1}{2}}\left(h_{i,j,k+1}^{n-1} - \mathrm{TOP}_{i,j,k+1}\right) \tag{9.6.16}$$

where q_c^n is the value of q_c added to the right side of Equation 9.5.24 in the nth iteration and $h_{i,j,k+1}{}^{n-1}$ is the head from the preceding iteration.

9.6.5 Solver Packages

The four solver packages in the MODFLOW-2000 are (1) the strongly implicit procedure (SIP),[39] (2) the slice successive over-relaxation (SOR),[39] (3) the preconditioned conjugate gradient (PCG),[24] and (4) the direct solution based on alternating diagonal ordering (DE4).[19] A detailed discussion of these various solvers is beyond the scope of this book. Interested readers should refer to the noted references.

9.6.6 Telescopic Mesh Refinement

Telescopic mesh refinement in groundwater flow modeling is an approach to use a larger (regional) encompassing model to define the boundary conditions and model parameters for a smaller (local) embedded model.[34] (Also refer to Buxton and Reilly[8] and Ward et al.[63] for more detail and applications of the approach.) This method is used when a detailed model is needed for a relatively small area as compared to the entire aquifer system, such the analysis of well fields[42] and contaminant plumes.[63] Essentially, the approach can be used to construct a detailed model from a larger (regional) groundwater flow model and can be used repeatedly to construct successively smaller (local) embedded models, hence the name "telescopic" mesh refinement.

Leake and Claar[34] discuss two basic approaches to construct data for local groundwater models. The first approach is to use a telescopic mesh refinement program such as MODTMR (*MOD*FLOW *T*elescopic *M*esh *R*efinement), which constructs the data set for the perimeter boundary conditions of a local model using cell-by-cell terms and head values in a regional model. This model can construct embedded-model data sets for most of the MODFLOW packages. A second approach is to use a manual-gridding process, a geographic information system (GIS), or other data processing programs to construct local-model data sets from grid-independent data. The first approach can provide maximum consistency between the local and regional model and would require less effort than the second approach, which has the main advantage in that local-model data sets are most consistent with locations and distributions of aquifer properties and sources and sinks contained in the grid-independent data sets. Two other programs have been developed by the U.S. Geological survey. TMRDIFF (*T*elescopic *M*esh *R*efinement *DIFF*erence) constructs files with comparisons of computed heads or drawdowns in the local model with computed heads or drawdowns in the regional model. RIVGRD constructs MODFLOW input data files for the River Package, the Drain Package, the General-Head Boundary Package, and the Stream Package.[53]

Figure 9.6.8 illustrates the telescopic mesh refinement modeling approach. Figures 9.6.9 and 9.6.10 illustrate the application of this approach to a hazardous waste site in the Miami River Valley near Dayton, Ohio. Ward et al.[63] used a nested series of three models designed on the regional, local, and site scales. Note that the grid for the site model is oriented differently than the local scale and regional models.

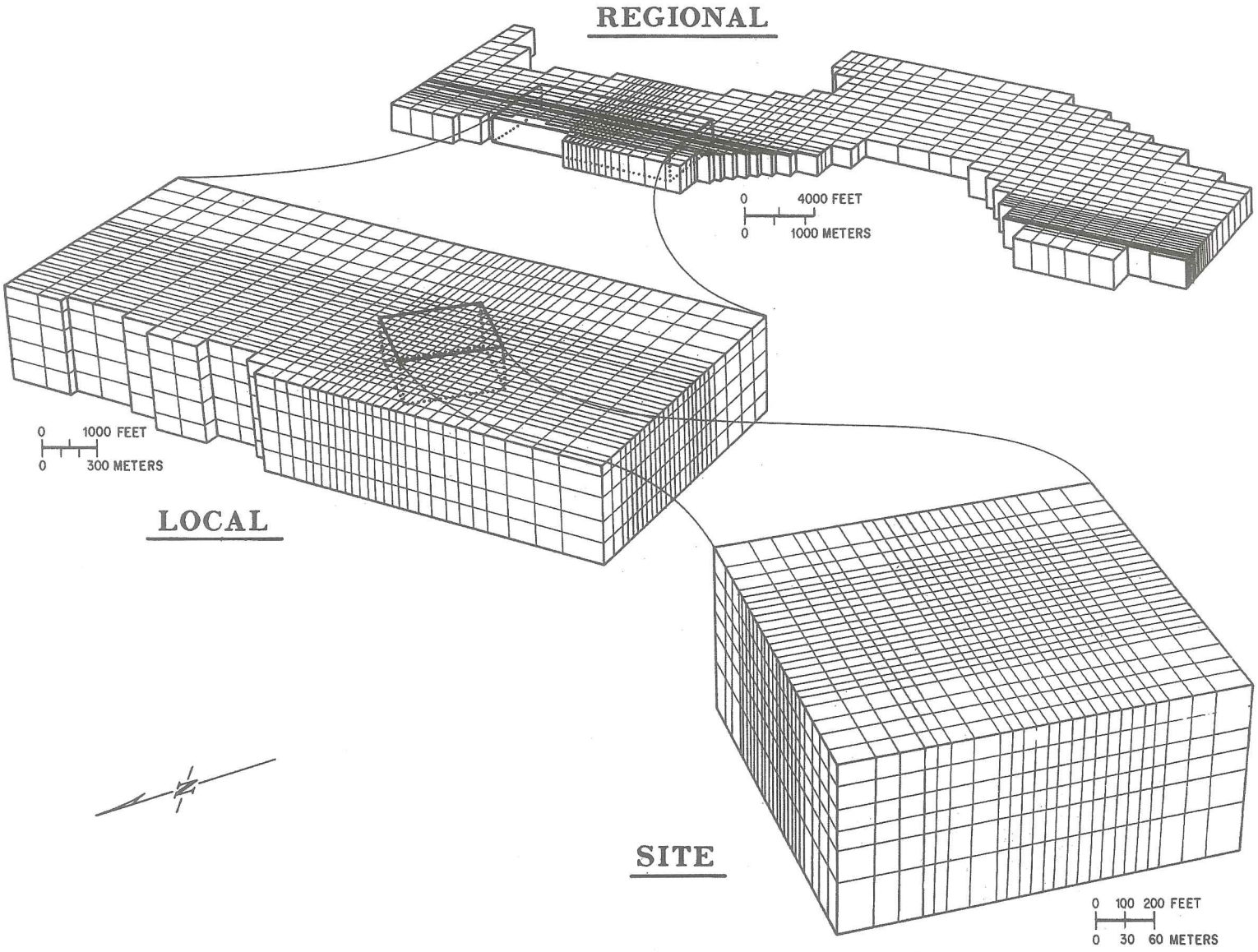

Figure 9.6.8. Conceptual diagram of the telescopic mesh refinement modeling approach (Ward et al.[63]).

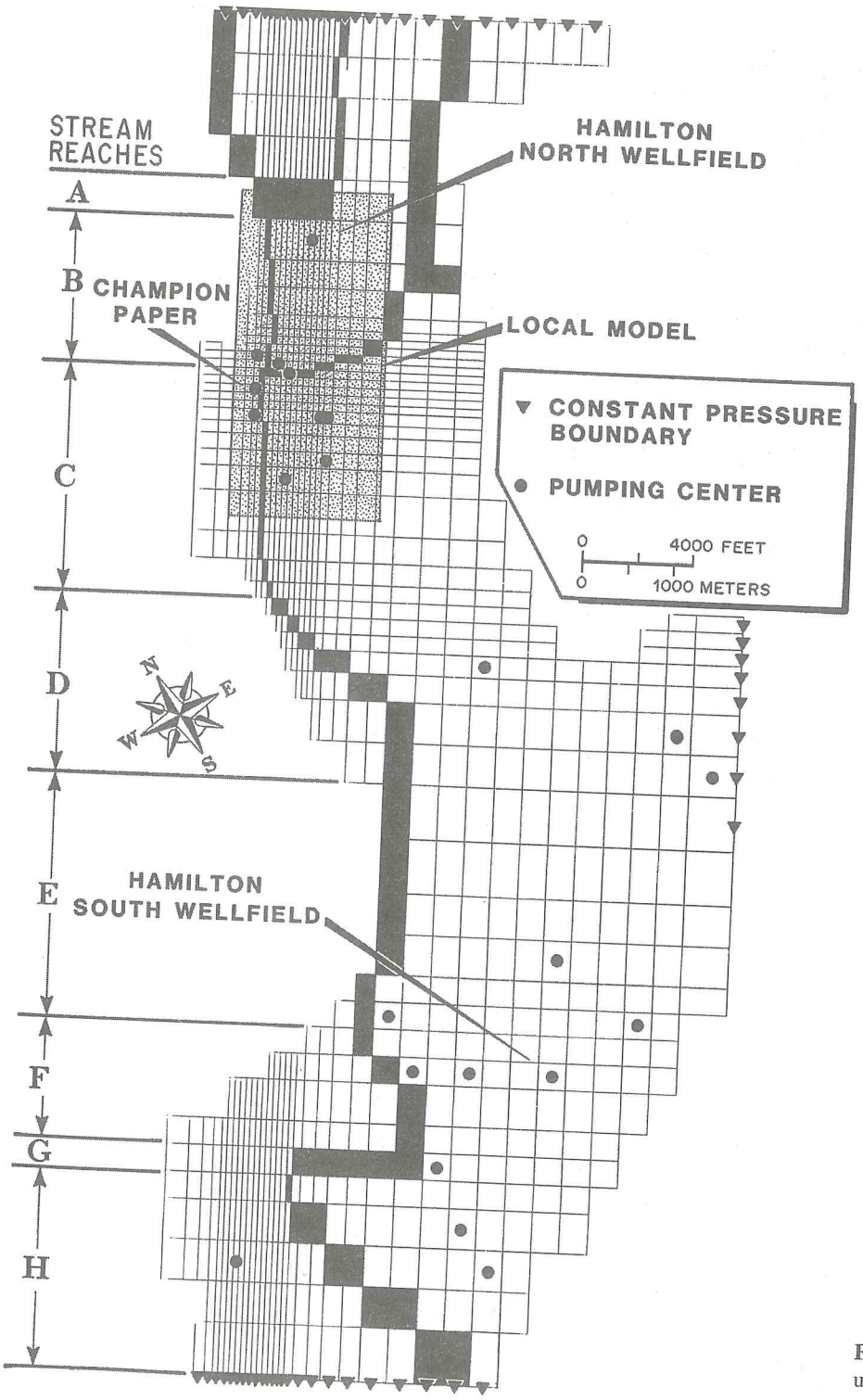

Figure 9.6.9. Finite difference grid used for the regional scale flow model of the Great Miami River Valley-Fill Aquifer.[63]

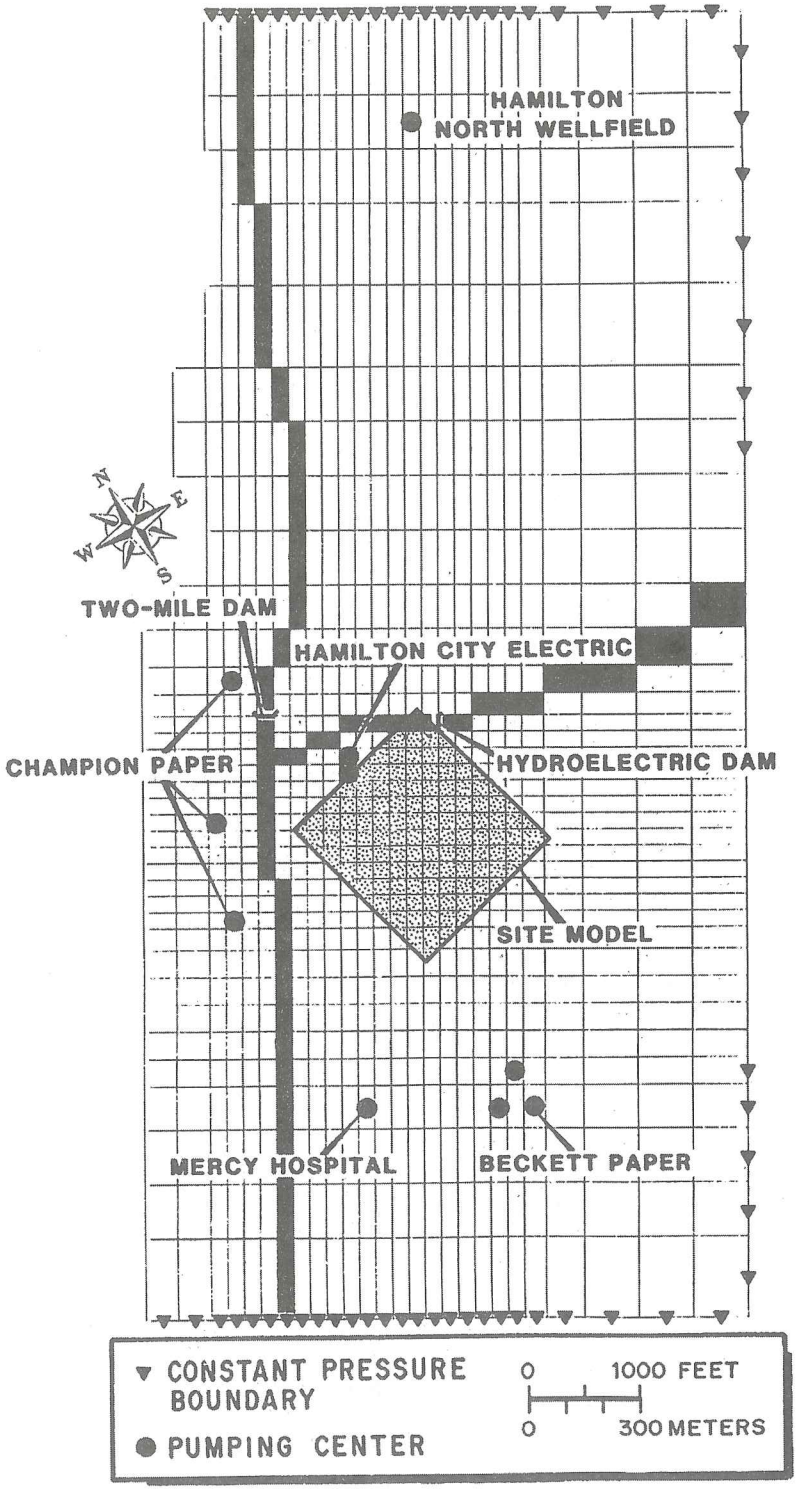

Figure 9.6.10. Finite difference grid used for the local-scale flow model of the Great Miami River Valley-Fill Aquifer. Relationship to regional-scale model is shown in Figure 9.6.9.[63]

9.7 CASE STUDY *Using MODFLOW: Lake Five-O, Florida*

MODFLOW is used widely in the United States and throughout the world by consultants and government agencies. The U.S. Geological Survey, as well as many other federal and state government agencies, use this program extensively and have applied it to many modeling applications. A few of the many applications by the U.S. Geological Survey include Belitz and Phillips,[7] Grubbs,[16] and Prince et al.[52]

The hydrologic budget for Lake Five-O in northwestern Florida (location shown in Figure 1.6.4) by Grubbs[16] was introduced in Chapter 1. The data-collection sites for the study area are shown in Figure 1.6.5. A three-dimensional model was developed by Grubbs[16] to represent the Lake Five-O groundwater system under steady-state and transient conditions.

9.7.1 Finite Difference Grid and Boundary Conditions

A finite difference grid was developed to approximate the geometry of the major lithologic contacts and aquifer boundaries. The areal discretization (81 rows and 57 columns) and boundary conditions for the models are illustrated in Fig. 9.7.1. All the rows in the grid have a width of 20 m. Columns 4 through 1 progressively increase in size westward from 30 to 100 m (expansion factor of 1.5). Columns 7 through 57 have a constant width of 20 m. The vertical discretization and boundary conditions are illustrated in Fig. 9.7.2. In the vertical, the sediments from the land surface to the uppermost part of the Upper Floridan aquifer were modeled using seven horizontal layers of varying thickness. Layer 1 was modeled as a water table layer; layers 2–6 were modeled as confined layers; and layer 7 was modeled as a specified boundary representing the Upper Floridan Aquifer.

Figure 9.7.2 presents the calibrated values of the hydraulic conductivity for the parameter zones used to represent variations in hydraulic properties. A single value or limited number of values of the hydraulic properties were assigned to parameter zones representing the lithologic units in order to approximate the surficial aquifer and intermediate confining unit. The following parameter zones were used by Grubbs:[16]

Basal clay zone—to represent the dense, low-permeability clay at the base of the intermediate confining unit;

Plateau zone—to represent increased anisotropy in the upper 5 to 10 m of the intermediate confining unit in the plateau area;

Transition zone—to represent the geometry of the contact between the surficial aquifer and intermediate confining unit where this contact dips toward the breaches in the intermediate confining unit;

Lakebed sediment zone—to represent lower permeability sediments (relative to the surficial aquifer) in surficial aquifer cells contiguous with and beneath the lake in model layers 3 and 4;

Lake Five-O—represented by a zone of highly conductive material in layers 1–4 and for transient simulations. The storage properties of the lake zone are identical to those of water.

The within-layer variations in horizontal hydraulic conductivity were accounted for by using equivalent hydraulic conductivity values computed using a weighted mean algorithm (Freeze and Cherry[11]). The transmissivity, T, of cells in the transition zone were computed using

$$T = LK_{h,eq} = L\left\{\frac{\left[\left(K_{h,SA}\right)\frac{L}{2}\right]}{L} + \frac{\left[\left(K_{h,ICU}\right)\frac{L}{2}\right]}{L}\right\}$$

$$= L\left(\frac{K_{h,SA}}{2} + \frac{K_{h,ICU}}{2}\right) \tag{9.7.1}$$

where L is the layer thickness, $K_{h,eq}$ is the equivalent horizontal hydraulic conductivity, and $K_{h,SA}$ and $K_{h,ICI}$ are respectively the horizontal hydraulic conductivities for the surficial aquifer and intermediate confining unit. The vertical flow between model layers was simulated using the leakance parameter (vertical hydraulic conductivity divided by flow path distance). In the cases when the vertical hydraulic conductivity varied within a model layer or across contiguous model layers, the leakance values were calculated with equivalent vertical hydraulic conductivities using the harmonic mean algorithm of Equation 9.5.2.

9.7.2 Model Calibration and Sensitivity Analysis

Four steady-state models were calibrated to the hydrologic conditions on four separate dates in 1988 to 1990 in order to satisfy one or more of the following objectives (see Grubbs[16]): (1) Refine the premodeling or prior estimates of hydraulic properties and their spatial distribution, (2) Provide initial conditions for transient simulations, and (3) Provide flow fields necessary for evaluation of flow paths and residence times of groundwater inflow into the lake. Calibration of the steady-state models was performed by comparing simulated and observed heads, and by comparing simulated lake seepage with minimum leakage estimates from hydrologic budget calculations (see Section 1.6 for the hydrologic budget and see Grubbs[16] for more detail on the calibration).

Calibration-sensitivity analysis of the steady-state model was performed by varying model input variables (within probable ranges) and comparing model outputs (simulate heads, lake inflow, and lake leakage) to known conditions. The root-mean-square error (RMSE) of the simulated heads to changes in horizontal hydraulic conductivity, leakance, recharge, and anisotropy

(*continues*)

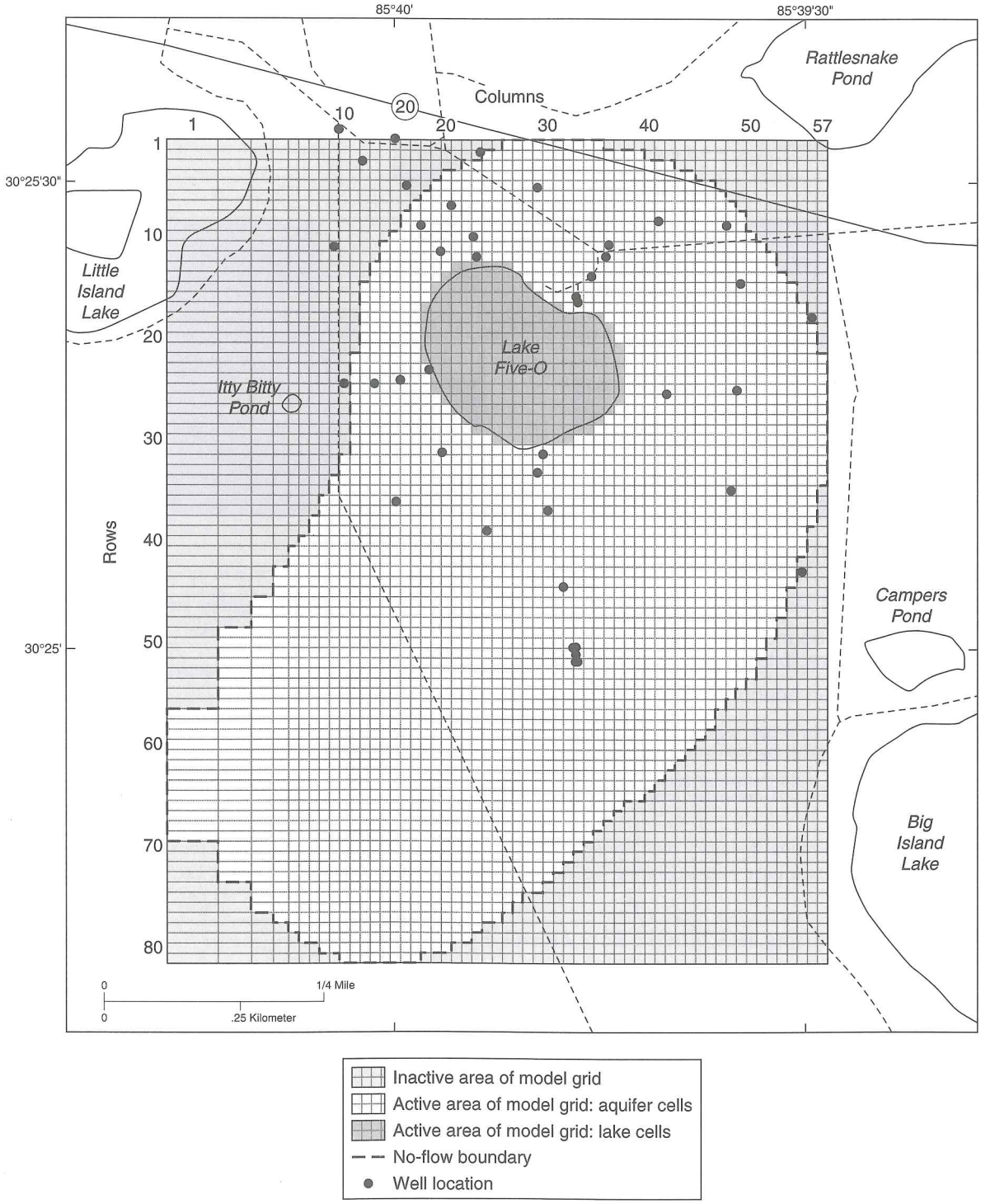

Figure 9.7.1. Areal discretization and boundary conditions for simulation models of the groundwater flow system near Lake Five-O (Grubbs[16]).

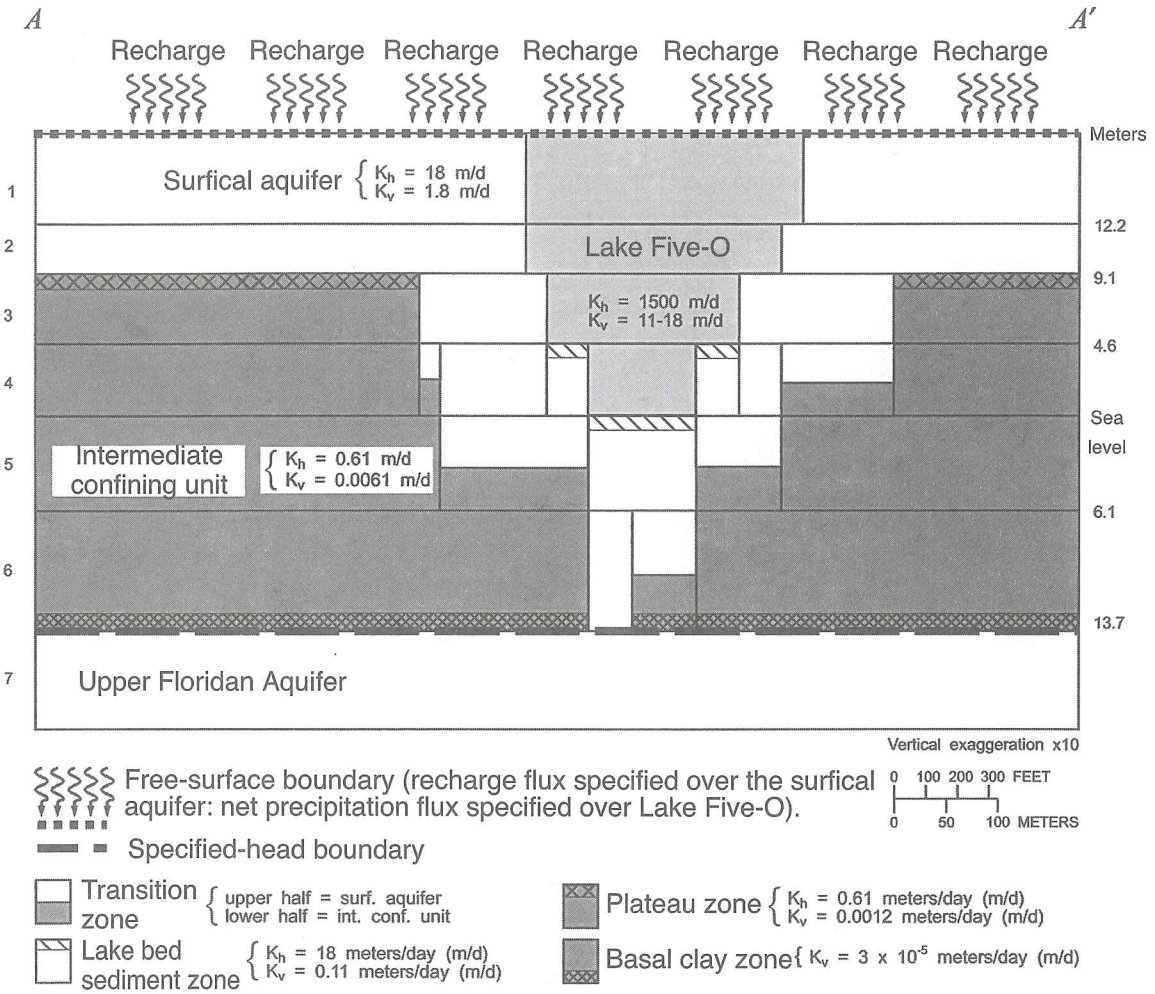

Figure 9.7.2. Vertical discretization, boundary conditions, and calibrated values of hydraulic conductivity for simulation models of the groundwater flow system near Lake Five-O(Grubbs[16]). Cross-section A-A′ location is shown in Figure 1.6.5.

9.7 CASE STUDY *Using MODFLOW: Lake Five-O, Florida (continued)*

are shown in Figures 9.7.3 and 9.7.4. The steep slope of the head-sensitivity curves (change from calibrated values versus RMSE) illustrate the sensitivity of the model to these variables. Head response was most sensitive to changes in recharge, horizontal hydraulic conductivity, and anisotropy of the surficial aquifer, and in horizontal hydraulic conductivity of the intermediate confining unit.

Transient model calibration determined storage properties and temporal changes in recharge rates. Hydraulic conductivities determined from the calibrated steady-state model calibrations were used in the transient model. The simulation period was divided into 43 stress periods. Assigned to each stress period were recharge rates, net precipitation rates, and beginning and ending heads to each stress period. First the specific yield in layer 1 and the specific storage in layers 2–6 were adjusted to simulate the slope of well hydrographs. Recharge was negligible during the calibration period selected because of below-normal rainfall, which made it possible to calibrate specific yield and specific storage independent of recharge. Sensitivity of the transient model to specific yield and specific storage is illustrated in Figure 9.7.5. The model is more sensitive to changes in specific yield than to changes in specific storage.

(*continues*)

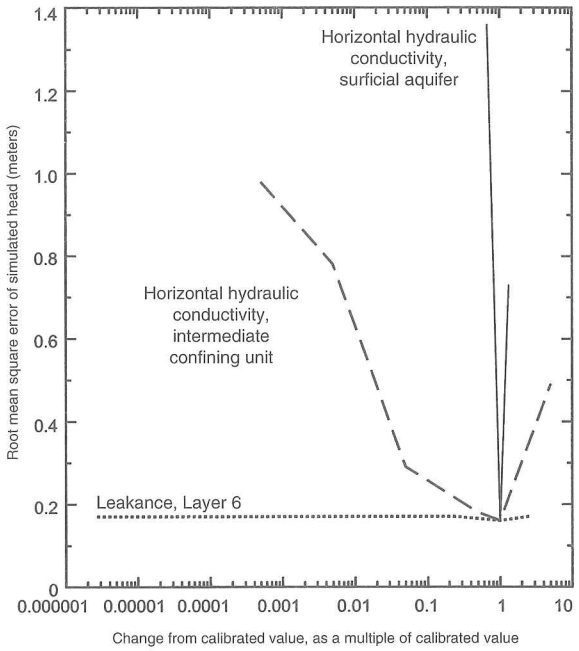

Figure 9.7.3. Sensitivity of steady-state models of groundwater flow system near Lake Five-O to changes in horizontal hydraulic conductivity and leakance of layer 6 (Grubbs[16]).

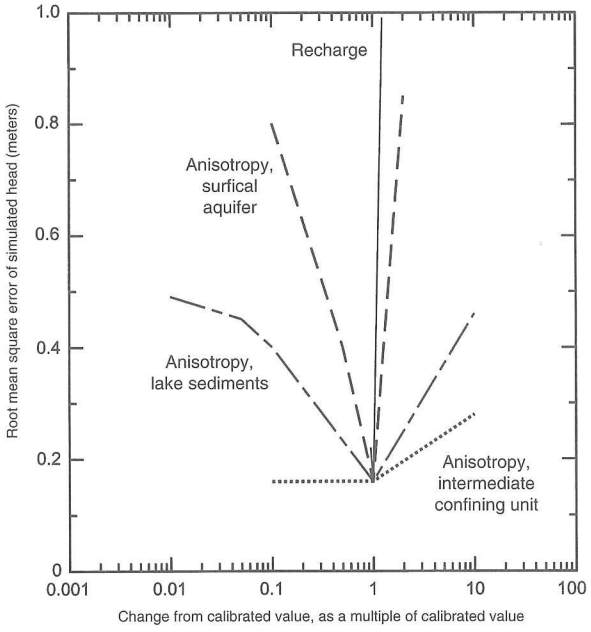

Figure 9.7.4. Sensitivity of steady-state models of groundwater flow system near Lake Five-O to changes in recharge and anisotropy (Grubbs[16]).

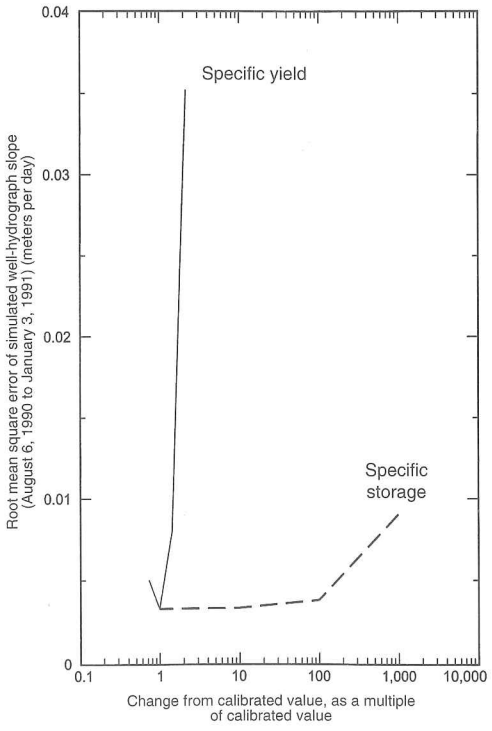

Figure 9.7.5. Sensitivity of transient model of the groundwater flow system near Lake Five-O to changes in aquifer storage properties (Grubbs[16]).

9.7 CASE STUDY *Using MODFLOW: Lake Five-O, Florida (continued)*

The calibration of recharge consisted of adjusting the recharge function to reproduce well hydrographs and monthly estimates of the net groundwater flow. The recharge function used by Grubbs[16] is

$$R_{\Delta t} = S_y \left[\int_{\Delta t} \dot{h}(t)dt + \bar{h}_{\text{recess}} \Delta t \right] \tag{9.7.2}$$

where $R_{\Delta t}$ is the recharge over time interval Δt, S_y is the specific yield, and $\bar{h}_{\text{recess}}$ is the absolute value of the average change in water table during a given hydrograph recession under suitably dry conditions. Simulated and measured heads are shown in Figure 9.7.6. Simulated and computed net groundwater flows to Lake Five-O are shown in Figure 9.7.7.

9.7.3 Model Results

Grubbs[16] concluded that the model simulations indicated that the groundwater system is the dominant source of water for Lake Five-O and that the groundwater system is the dominant sink for water leaving Lake Five-O. In fact, the simulated groundwater inflow and leakage were approximately four and five times larger than precipitation inputs and evaporative losses, respectively, during the calendar years 1989–1990. Spatial distributions of simulated groundwater inflow and leakage showed little variation between wet and dry periods.

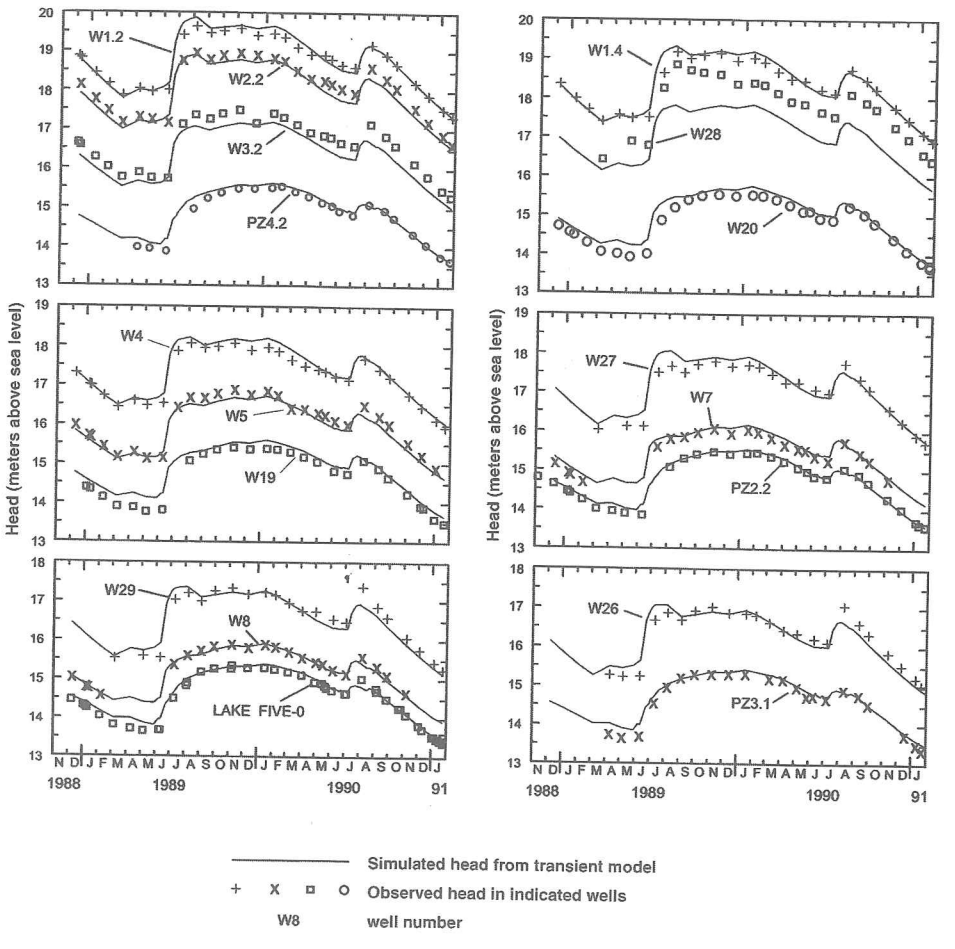

Figure 9.7.6. Simulated and observed heads for Lake Five-O and adjacent groundwater system, December 12, 1988, through January 22, 1991 (Grubbs[16]).

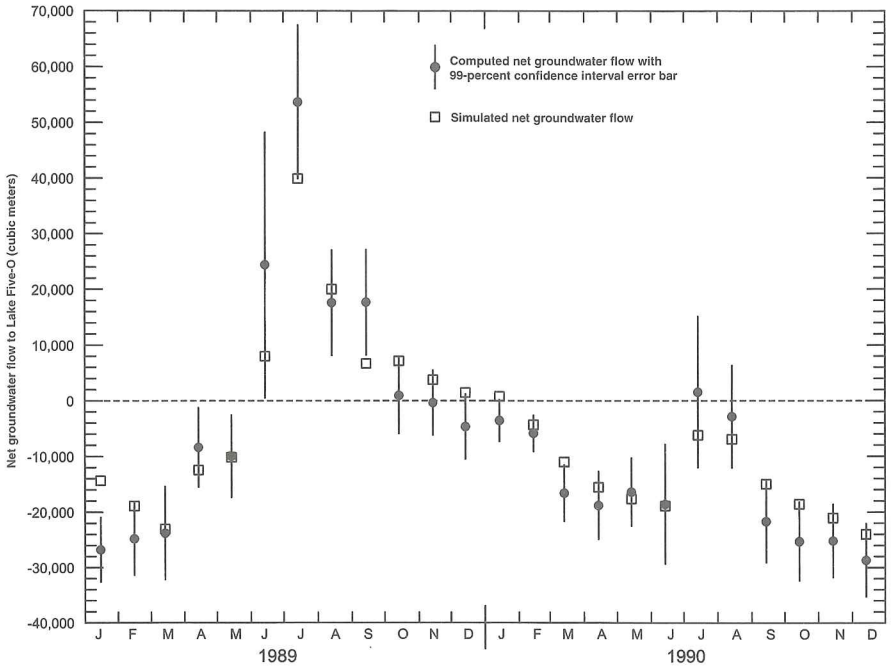

Figure 9.7.7. Simulated and computed monthly net groundwater flow to Lake Five-O, 1989–90 (Grubbs[16]).

9.8 PARTICLE TRACKING—MODPATH

9.8.1 What Is Particle Tracking?

Particle tracking is used to trace out flow paths, or path lines, by tracking the movement of infinitely small imaginary particles placed in the flow field.[4] Particle tracking computer programs, such as the MODPATH,[46–48] are postprocessors to MODFLOW. MODPATH accepts the head distribution from MODFLOW and uses it to compute the velocity distribution,[12] which is then used to trace out path lines. Particle tracking can be used to help visualize the flow field and to track contaminant paths. Anderson and Woessner[4] also point out that particle tracking analysis should be used routinely with groundwater flow modeling to detect conceptual errors that cannot be detected solely by examining the head distribution. Particle tracking analysis can be used to evaluate the effects of different boundary conditions and can show the location of recharge and discharge more clearly than results from groundwater flow models.

9.8.2 Particle Tracking Analysis—An Application

Grubbs[16] used the particle tracking code by Pollock[47] to evaluate the groundwater path lines (flow paths) and residence times for hypothetical parcels of groundwater (particles) that discharge to Lake Five-O in northwestern Florida. Figures 9.8.1 and 9.8.2 illustrate the results of the particle tracking. Figure 9.8.1 indicates that most of the surrounding groundwater basin contributes to flow into the lake. According to Grubbs,[16] the *residence times* (travel time of the inflow particles from recharge at the water table to discharge at the lake) generally ranged from 0.6 to 9 years, with mean residence times ranging from 3 to 6 years. Also, there was very little variation in these residence times between high and low water conditions.

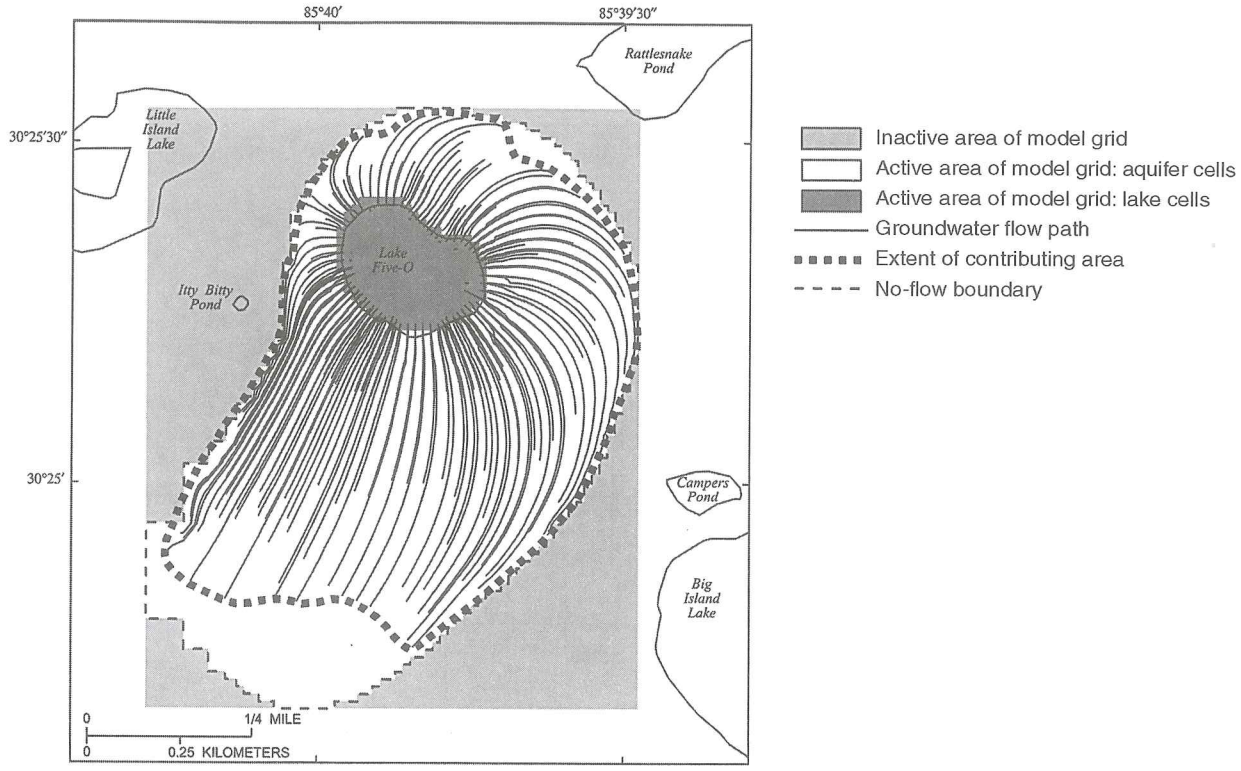

Figure 9.8.1. Contributing area to Lake Five-O, as defined by groundwater flow paths of particles that discharge to the lake (Grubbs[16]).

The flow paths in Figure 9.8.2 illustrate the vertical character of the groundwater flow within and between the surficial aquifer and intermediate confining unit. Flow lines are deflected downward at two stagnation points, a very small distance outside the lakebed. These are locations where the head in the groundwater flow is the same as the altitude of the lake surface. At these two points, groundwater flow into the lake and leakage from the lake to the groundwater occur below these points. According to Grubbs,[16] the location of these two points did not change much from low to high water conditions. Flow paths in Figure 9.8.2 indicate that most all of the groundwater flow near Lake Five-O occurs within the surficial aquifer. In addition the groundwater that discharges into the lake does not move through the intermediate confining unit.

9.9 EXAMPLE APPLICATIONS AND INPUT OF MODFLOW

EXAMPLE 9.9.1

TWO-DIMENSIONAL STEADY-STATE PROBLEM

Consider the aquifer (uniformly discretized into cells of 500 ft × 500 ft) shown in Figure 9.9.1, with specified head boundaries along row 1 and along column 7. Think of this as two rivers intersecting perpendicularly in the northeastern corner of the modeled groundwater system. A single aquifer is being modeled so that only one layer is required. The aquifer is treated as a confined aquifer because of its relative thickness and because it does not experience large changes in saturated thickness. The transmissivity of the aquifer is 500 ft^2/d and it recharges at a rate of 0.001 ft/d. A well is located at row 5, column 3, which discharges at a rate of 8,000 ft^3/d. Heads for all the active cells are set at 10 ft. A time step of 365 days is to be used.

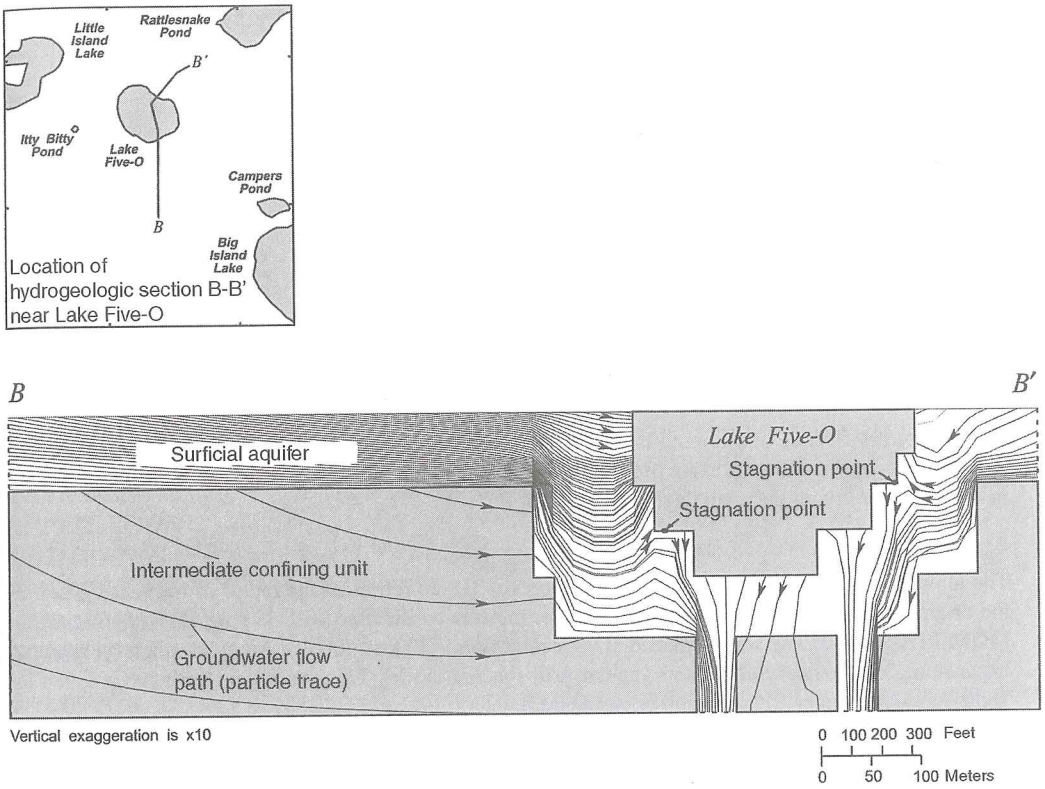

Figure 9.8.2. Particle traces projected onto hydrogeologic section B–B′ near Lake Five-O (Grubbs[16]).

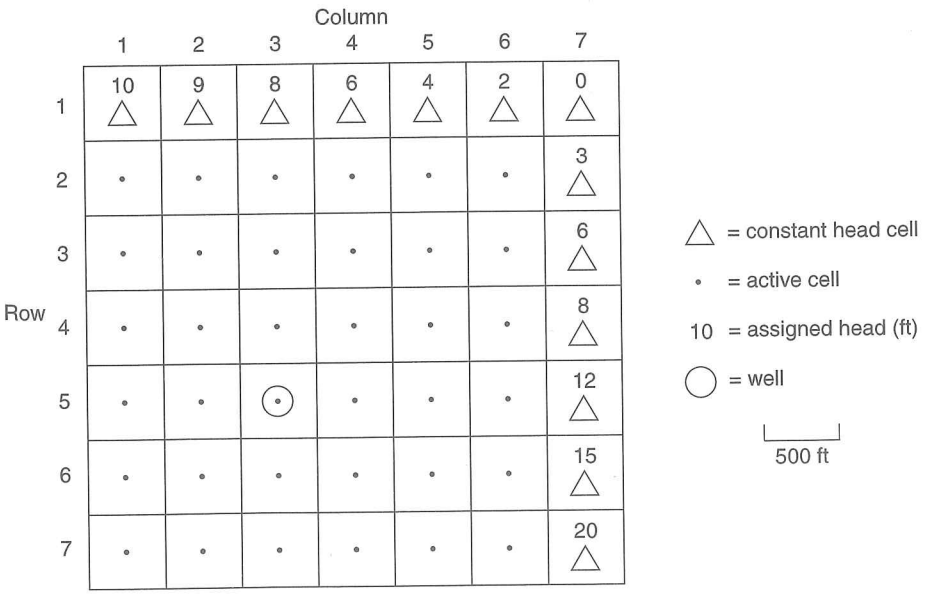

Figure 9.9.1. Example 9.9.1 aquifer discretization with 500 ft × 500 ft cells.

The MODFLOW model input data is presented in Table 9.9.1 (Appendix B) with brief explanations of the input. The strongly implicit procedure (SIP) solution technique is used and a maximum of 50 iterations (MXITER) is specified. The number of iteration parameters (NPARM) is 5, the acceleration

number (ACCL) is 1, the head change criterion is 0.01, IPCALC = 1, WSEED = 0, and IPRSIP = 1. See the MODFLOW input manual for detailed descriptions of the input.

SOLUTION

Output data are given in Table 9.9.2 (Appendix B).

EXAMPLE 9.9.2

STEADY-STATE APPLICATION COMPARING ANALYTICAL AND NUMERICAL SOLUTIONS

This example uses MODFLOW model for a steady-state problem in a confined aquifer. The aquifer is the same as described in Example 4.2.2:

$$K = 16.43 \text{ m/day}$$

$$b = 10 \text{ m}$$

$$r_w = 0.5 \text{ m}$$

$$Q = 425 \text{ m}^3/\text{day}$$

The radius of influence of pumping is at 300 m from the pumping well. Construct a numerical model under steady-state conditions using MODFLOW, calculate the drawdown curve from $r = 0$ m to $r = 300$ m and compare it with the analytical (Thiem) solution.

SOLUTION

The input data are presented in Table 9.9.3 (Appendix B). To represent the radius of influence given in the original problem, a 600 m × 600 m one-layer mesh is constructed with 19 rows and 19 columns in MODFLOW model. The well is placed at the center point (300 m, 300 m). An increasing grid spacing expansion gives better results than a regular grid spacing model. The grid spacing scheme is given in Table 9.9.4 (Appendix B) and is shown in Figure 9.9.2.

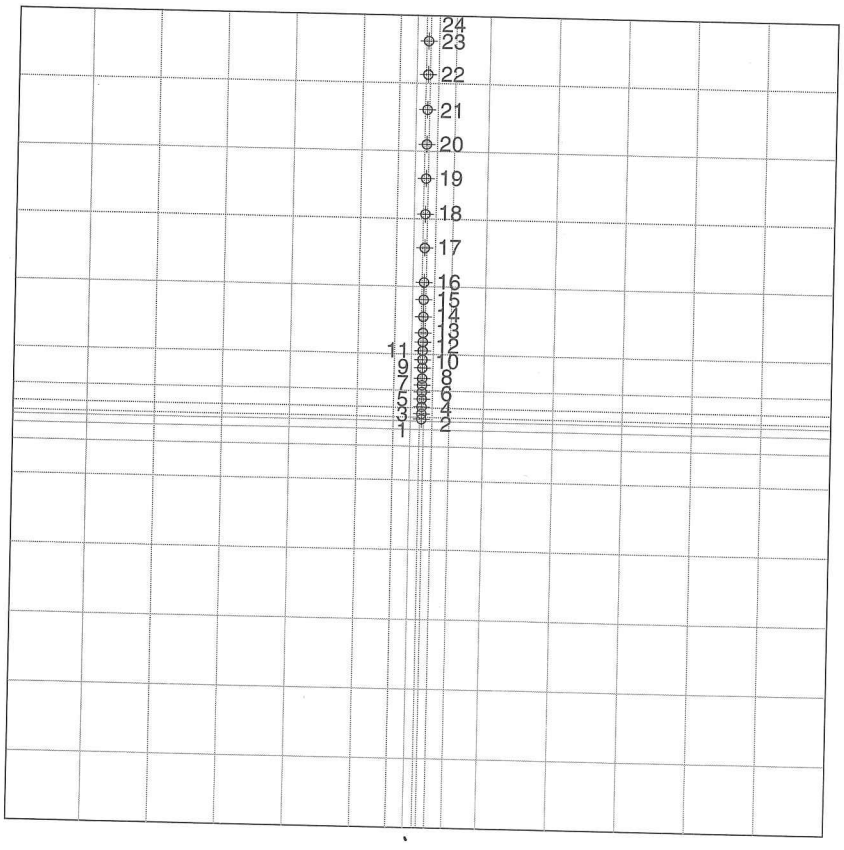

Figure 9.9.2. Grid-1 scheme used for Example 9.9.2.

The layer type is 0: *confined.* The *Transmissivity* flag is set to *User-specified.* The boundaries of the model are defined as *fixed-head boundaries.* A homogeneous transmissivity of 164.3 m/day is specified over the model domain. To calculate the drawdown curve, 27 boreholes are defined along a radial direction from $r = 0.5$ m to $r = 300$ m. The pumping well is placed at the center of the domain, row 10, column 10, with a pumping rate of 425 m^3/day. Simulation flow type is set to steady-state. See Table 9.9.5 (Appendix B) for output.

The resulting drawdown curves from the analytical (Thiem) and numerical (MODFLOW) solutions are given in Table 9.9.6 (Appendix B) and plotted in Figure 9.9.3.

The MODFLOW results compare well to the analytical solution. The numerical results of the given problem are within 0.05 m of the analytic results except near the pumping well (0.5 m $< r <$ 8 m). An exact comparison is not attained because of the use of a discrete rather than continuous spatial domain. It should also be remembered that the radius of influence in the original problem, $r = 300$ m, is approximated by setting the boundaries of the square model domain as fixed-head boundaries. ■

EXAMPLE 9.9.3

TRANSIENT APPLICATION COMPARING ANALYTICAL AND NUMERICAL SOLUTIONS

Using the data given in Example 4.4.4, construct a one-layer model in MODFLOW and calculate the drawdown vs. time curve 50 m away from the pumping well for $t = 0$ to $t = 1$ day. Compare the numerical results to the analytical solution of Theis.

SOLUTION

The aquifer given in Example 4.4.4 is confined with the following supplemental data:

$$b = 12 \text{ m}$$

$$K = 25 \text{ m/day}$$

$$S = 0.0001$$

$$Q = 300 \text{ m}^3\text{/day}$$

The exact analytical solution of the problem (using Theis) is also given below for comparison. Two different grid spacing schemes are used in the MODFLOW model listed in Table 9.9.7 (Appendix B).

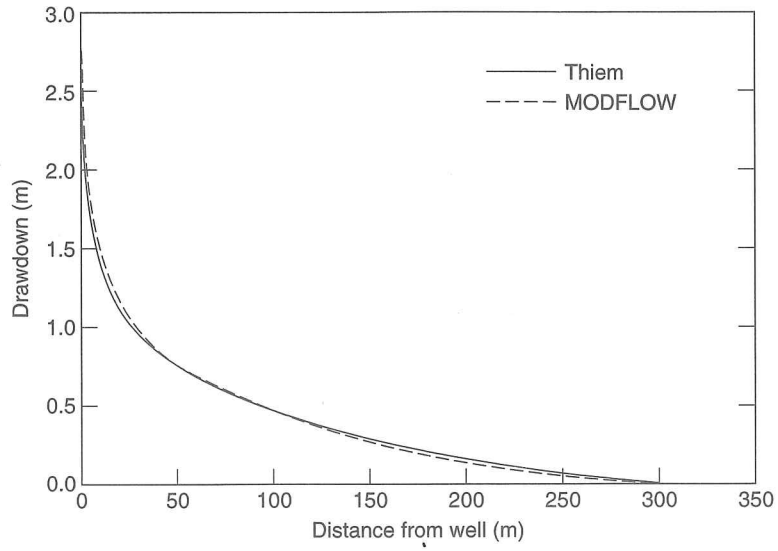

Figure 9.9.3. Example 9.9.2: Comparison of distance versus drawdown for the Thiem equation and MODFLOW.

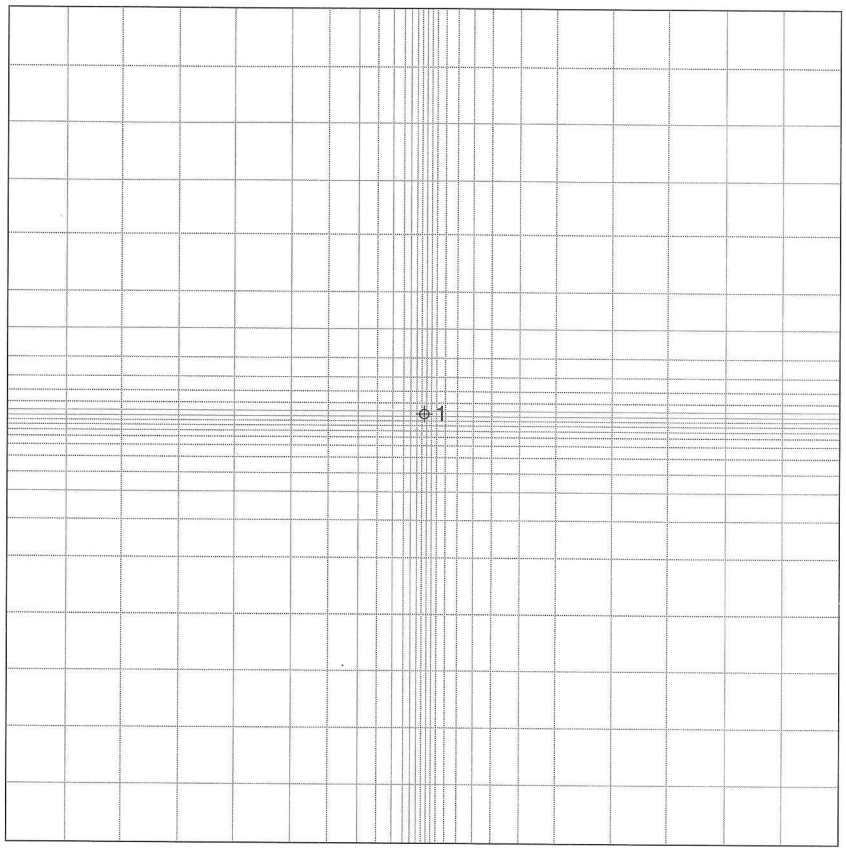

Figure 9.9.4. Grid-2 model scheme for Example 9.9.3.

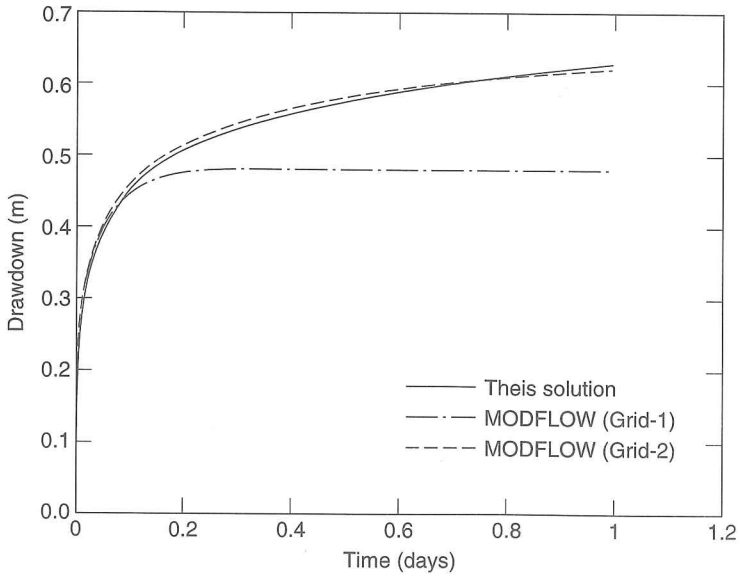

Figure 9.9.5. Example 9.9.3: Comparison of time-drawdown for the Theis equation and MODFLOW.

Grid-1 covers a square area of 2,000 m × 2,000 m and consists of 19 rows and 19 columns. An increasing grid spacing is used as shown in Table 9.9.7. Grid-2 (Figure 9.9.4) is an expanded version of Grid-1 with 29 rows and 29 columns covering an area of 5,000 m × 5,000 m. The simulation time is set to one day with

20 time steps and a time step expansion factor of 1.3. The SIP package is used as the model solver with five iteration parameters, 0.0001 as the closure criterion, and the maximum number of iterations is set to 50.

The resulting drawdown curves 50 m away from the pumping well using the Theis solution and MODFLOW model are illustrated in Figure 9.9.5. The artificial fixed head boundaries of the Grid-1 model start to affect the drawdown curve at 50 m approximately 0.1 day after the pumping starts. To meet the requirement of an infinite aerial extent aquifer, inherent in the Theis solution, the fixed head boundaries are moved farther away from the pumping well in the Grid-2 model. With this modification, the effect of the boundaries are not observed at 50 m for the given time period ($0 < t < 1$). The MODFLOW results using Grid-2 compare well to the analytic solution. The numerical results are generally within 1 cm of the analytic solution. ■

9.10 SOLUTE TRANSPORT MODELING—MOC3D

9.10.1 Solute Transport Equation

The solute transport equation[32] is

$$\frac{\partial(\varepsilon C)}{\partial t}+\frac{\partial(\rho_b \overline{C})}{\partial t}+\frac{\partial}{\partial x_i}(\varepsilon C V_i)-\frac{\partial}{\partial x_i}\left(\varepsilon D_{ij}\frac{\partial C}{\partial x_j}\right) - \sum C' W+\lambda(\varepsilon C+\rho_b \overline{C})=0 \tag{9.10.1}$$

(summation over repeated indices is understood), where C is volumetric concentration (mass of solute per unit volume of fluid, ML^{-3}), ρ_b is the bulk density of the aquifer material (mass of solids per unit volume of aquifer, ML^{-3}), $\overline{C}$ is the mass concentration of solute sorbed on or contained within the solid aquifer material (mass of solute per unit mass of aquifer material, MM^{-1}), ε is the effective porosity (dimensionless), V is a vector of interstitial fluid velocity components (LT^{-1}), D is a second-rank tensor of dispersion coefficients (L^2T^{-1}), W is a volumetric fluid sink ($W < 0$) or fluid source ($W > 0$) rate per unit volume of aquifer (T^{-1}), C' is the volumetric concentration in the sink/source fluid (ML^{-3}), λ is the decay rate (T^{-1}), t is time (T), and x_i are the Cartesian coordinates (L).

The terms controlling sorption are combined into a single parameter—the retardation factor (R_f), which is assumed to be constant in time because on a linear isotherm, $C/\overline{C}$ is constant. The *retardation factor* is defined as

$$R_f = 1+\frac{\rho_b \overline{C}}{\varepsilon C}. \tag{9.10.2}$$

A number of the assumptions that follow are made in the development of the governing equations.[32]

1. Darcy's law is valid, and hydraulic head gradients are the only significant driving mechanism for fluid flow.
2. The hydraulic conductivity of the aquifer system is constant with time. Also, if the system is anisotropic, it is assumed that the principal axes of the hydraulic-conductivity tensor are aligned with the coordinate system of the grid, so that the cross-derivative terms of the hydraulic-conductivity tensor are eliminated.
3. Gradients of fluid density, viscosity, and temperature do not affect the velocity distribution.
4. Chemical or biological reactions do not affect the fluid or aquifer properties.
5. The dispersivity coefficients are constant over a flow time step, and the aquifer is isotropic with respect to longitudinal dispersivity.

The solution of the transport equation requires knowledge of the velocity (or specific discharge) field. After the head distribution has been calculated for a given time step or steady-state flow condition, the specific discharge across every face of each finite difference cell within the transport subgrid is calculated using a finite difference approximation.[32]

The mass-tracking algorithm requires that the seepage velocity at any point within a cell be defined to compute advective transport. Seepage velocity is calculated at points within a finite difference cell based on linearly interpolated estimates of specific discharge at those points divided by the effective porosity of the cell.[32]

9.10.2 MOC3D Model

MOC3D is a general-purpose computer model developed by the U.S. Geological Survey for simulation of three-dimensional solute transport in groundwater (see references 13, 14, 15, 23, 27, 29, 32, and 41 for more detail). This model computes changes in concentration of a single dissolved chemical constituent over time that are caused by advective transport, hydrodynamic dispersion (including both mechanical dispersion and diffusion), mixing (or dilution) from fluid sources, and mathematically simple chemical reactions (including linear sorption, which is represented by a retardation factor, and decay). MOC3D can be used to simulate groundwater age transport and the effects of double porosity and zero-order growth/loss. The model uses the method of characteristics to solve the transport equation on the basis of the hydraulic gradients that are computed with MODFLOW for a given time step. Particle tracking is used to represent advective transport and explicit finite difference methods are used to calculate the effects of other processes.

The notation and conventions used in MOC3D to describe the grid and to number nodes are illustrated in Figures 9.10.1 and 9.10.2. The indexing notation used is consistent with that used in MODFLOW.

Application of MOC3D is the third step in a logical sequence of (1) flow, (2) advective transport, and (3) solute transport simulation as illustrated in Figure 9.10.3. After the flow

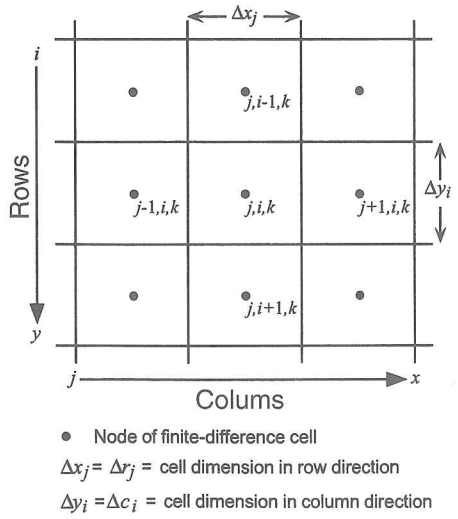

Figure 9.10.1. Notation used to label rows, columns, and nodes within one layer (k) of a three-dimensional, block-centered, finite difference grid for MOC3D.[32]

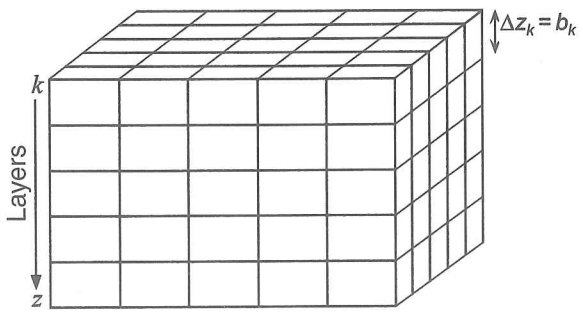

Figure 9.10.2. Representative three-dimensional grid for MOC3D illustrating notation for layers.[32]

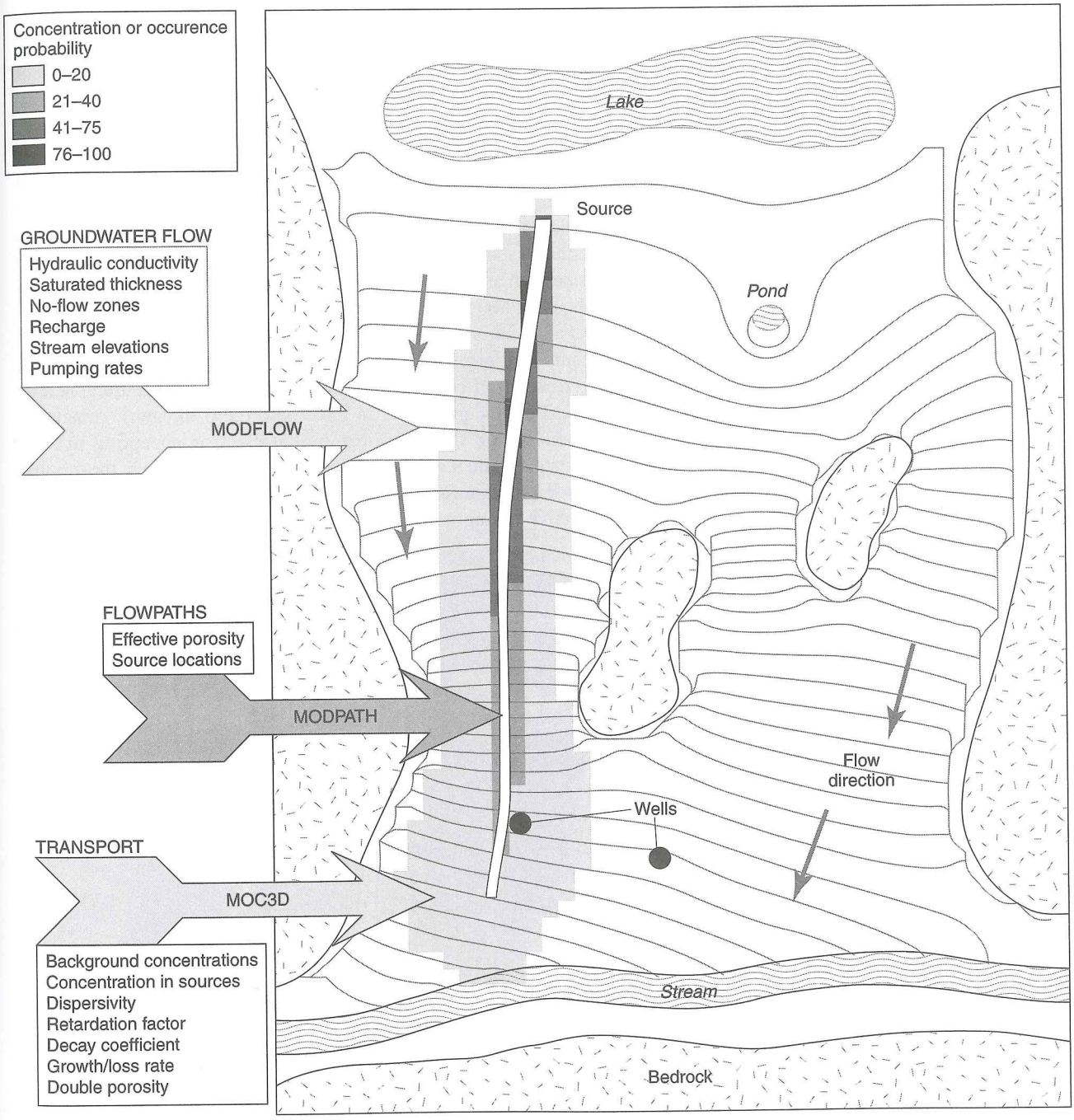

Figure 9.10.3. Typical input and illustration of output for simulation of groundwater flow and solute transport using MODFLOW, MODPATH, and MOC3D (Goode[14]).

model (MODFLOW) is constructed, advective transport can be modeled by particle tracking using MODPATH.[48] Because travel times are needed, the effective porosity must be specified. The solute transport as a result of advection and dilution (mixing) can be modeled using MOC3D using specified initial and source concentrations. Optional input on dispersion and reactions allows effects of these processes to be modeled. The simulation of solute transport

with dispersion using MOC3D can enhance particle-tracking analyses by approximating uncertainty in source–area delineation and potential contamination advection.[13, 14]

Figure 9.10.3 shows nine closely spaced pathlines of groundwater flow from a continuous source of contamination after 20 years. These were calculated using MODFLOW and MODPATH. MOC3D was used to simulate the dispersed plume from the same source location. This dispersed plume can be interpreted as the probability that the contaminant will be detected at each location within 20 years. As pointed out by Goode,[13] the dispersion coefficient approximately accounts for the uncertainty in predicted flowpaths caused by imperfect knowledge of aquifer properties, recharge rates, stream levels, and other factors. Detailed field characterization can reduce uncertainties and make the contaminant occurrence probability map more accurate. These approaches can also be used to delineate probabilistic source areas (capture zones) for pumping wells using MOC3D.

An example of a MOC3D application is illustrated in Figure 9.10.4, which uses time- and space-varying decay coefficients to approximate biodegradation of benzene at a Laurel Bay, South Carolina research site. Benzene attenuation depends on decay rates that are generally higher in aerobic (oxygen rich) zones and lower in anaerobic (zero oxygen). Anaerobic biodegradation rates are dependent on the specific terminal-electron-accepting process (TEAP) controlling the redox state. Figure 9.10.4a shows the TEAP zones. Also in the groundwater at this site is methyl *tert*-butyl ether (MTBE). This is also a gasoline-derived contaminant, but is essentially nonreactive during transport. Source concentrations are the same for

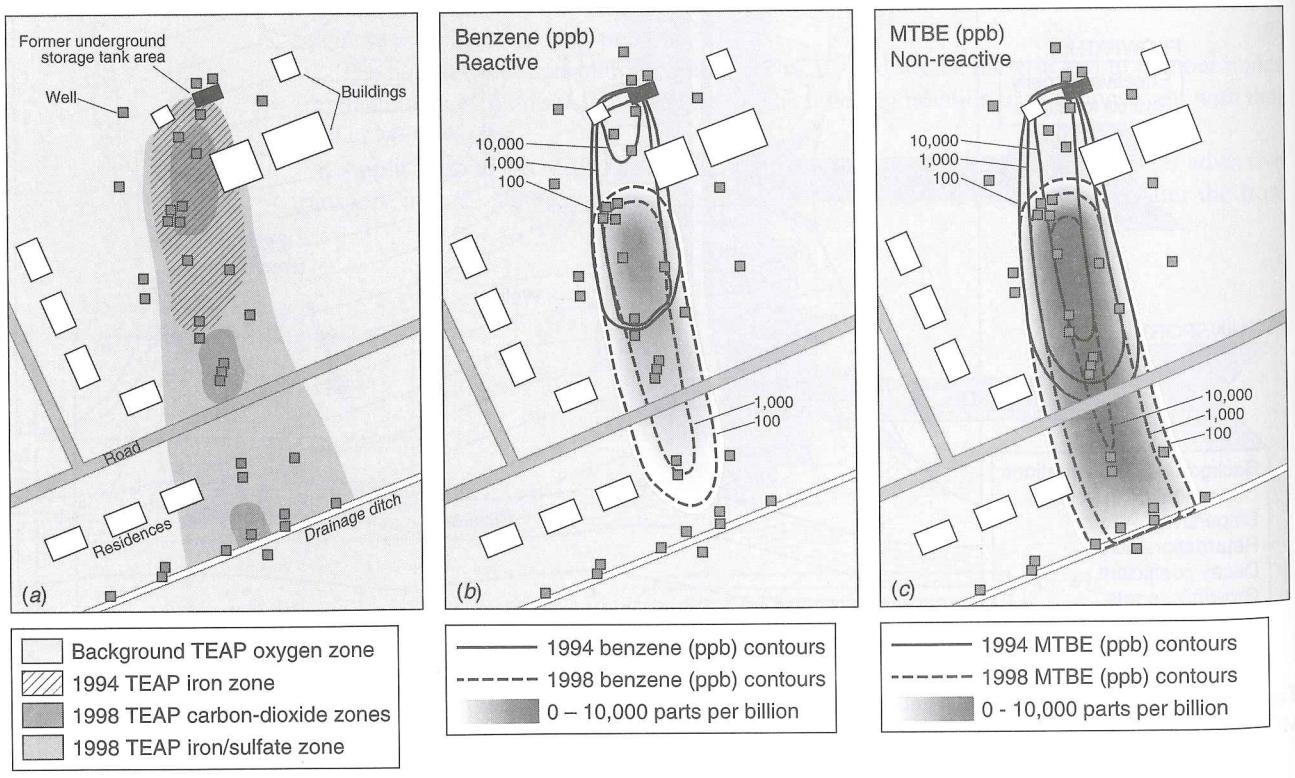

Figure 9.10.4. MOC3D simulation of benzene and MTBE at the Laurel Bay, SC, research site, based on field and lab data of Landmeyer[33] and others (1998): (*a*) Location map with anaerobic terminal-electron-accepting-process (TEAP) zones in 1994 (hatched) and 1998 (shaded); (*b*) Benzene in 1994 and 1998; (*c*) MTBE in 1994 and 1998. In (*b*) and (*c*), the 1998 shaded maps range from 0 to 10,000 parts per billion (ppb); contours show 100, 1,000, and 10,000 ppb concentration levels (as presented in Goode[14]).

both contaminants; therefore, differences in simulated concentrations result from differences in decay coefficients. Outside the TEAP zones fast aerobic degradation is taking place, except at the early time when microbes are assumed to be in low concentrations. This is illustrated by the differences in the 1994 and 1998 zones (see Figure 9.10.4a). Figure 9.10.4b show the results of MOC3D simulations of the benzene migration for 1994 to 1998 that has temporally and spatially varying decay coefficients. Figure 9.10.4c shows the results of MOC3D simulations of the MBTE for 1994 to 1998.

9.11 GROUNDWATER MODELING SOFTWARE SUPPORT

9.11.1 U.S. Geological Survey

The U.S. Geological Survey provides access to public-domain software, such as MODFLOW, MODPATH, MOC3D, and several other simulations models such as SUTRA for two- and three-dimensional variably saturated flow, solute or energy transport and several other computer models. ZONEBUDGET is a program for computing water budgets for MODFLOW. Access this software at http://water.usgs.gov/software/ground_water.html.

9.11.2 U.S. EPA Center for Exposure Assessment Modeling (CEAM)

The Center for Subsurface Modeling Support (CSMoS) provides public domain groundwater and vadose zone modeling software and services to public agencies and private companies. CSMoS is located at the National Risk Management Laboratory (NRML), U.S. EPA Center for Ground-Water Research, Ada, Oklahoma. Its primary aims are to provide direct technical support to EPA and state decision makers in subsurface modeling applications and to support the groundwater models and databases resulting from the research at NRML. A major focus of CSMoS is the coordination of the use of models for risk assessment, site characterization, remedial activities, wellhead protection, and Geographic Information Systems (GIS) application. The Web address for CSMoS is http://www.epa.gov/ada/csmos.html.

9.11.3 International Groundwater Modeling Center (IGWMC)

The International Ground Water Modeling Center (IGWMC) provides information, education, and research for groundwater modeling. It is located at the Colorado School of Mines, Golden, Colorado. IGWMC advises on groundwater modeling problems, distributes software, organizes short courses and workshops, and provides technical assistance on problems related to groundwater modeling. The Web address for IGWMC is http://www.mines.edu/igwmc/about.

9.11.4 Processors for MODFLOW

Because of the wide usage of the MODFLOW model, several pre and post-processing models have been developed. Some of the processors are PMWIN, Visual MODFLOW, MODFLOW-GUI PIE, and VIEWLOG. These processors can be located easily on the Internet by performing a search for their names.

PMWIN (see Chiang and Kinzelbach[9]) is a simulation package for pre- and post-processing that includes MODFLOW, MT3D, MT3DMS, PMPATH, UCODE, and PEST-LITE.

Visual MODFLOW, developed by Waterloo Hydrogeologic, Inc. of Ontario, Canada, is a pre-and post-processor for the MODFLOW and MODPATH models. This allows the user to solve the flow model and to perform particle tracking and velocity vector analysis. The program is completely graphical, allowing the user to input all necessary input parameters, run the program, and visualize the analysis results. The Visual MODFLOW package includes the

MODFLOW and MODPATH models and can import previously created MODFLOW data files. VIEWLOG is also a pre-and post-processor for the MODFLOW and MODPATH models.

MODFLOW-GUI PIE is a U.S. Geological Survey public domain GIS pre-and post-processor graphical-user interface for preparing MODFLOW, MOC3D, MODPATH, and ZONEBDGT input and viewing model output for use within Argus ONE. MODFLOW GUI PIE is used to graphically input GIS data, run MODFLOW, and visualize the results from within Argus ONE, which is an easy-to-use graphical workplace.

PROBLEMS

9.2.1 Explain the concepts of physical scale models, analog models, and mathematical models.

9.2.2 Discuss the concepts of porous media models, analog models, and electric analog models.

9.2.3 Discuss the theory upon which viscous fluid models are based.

9.2.4 Explain how electric analog models are used to model groundwater flow.

9.2.5 Explain how sand tank models are used to model groundwater flow.

9.2.6 Explain the concept of membrane models for groundwater flow.

9.2.7 Explain how Hele-Shaw models have been used in groundwater flow modeling.

9.2.8 Discuss in general the difference between the finite difference and finite element methods of groundwater modeling.

9.3.1 Discuss in detail the processes of calibration, calibration sensitivity analysis, and model verification and how they work together to develop a model.

9.3.2 Discuss in detail the processes of prediction and predictive sensitivity analysis in model development.

9.3.3 Develop a brief discussion of the various ASTM standards for groundwater flow modeling.

9.4.1 Show the development of Equation 9.4.10a.

9.5.1 Derive Equation 9.5.2 for the effective hydraulic conductivity.

9.5.2 Derive Equation 9.5.22, which is the finite difference approximation of the continuity for cell (i, j, k).

9.6.1 Derive Equation 9.6.10 for the calculation of conductance between nodes.

9.6.2 Derive Equation 9.6.12 for the calculation of vertical conductance between nodes.

9.9.1 Run the MODFLOW model for the problem in Example 9.9.1 using a time step of one day and a time step multiplier of 1.0. Compare the results with those obtained in Example 9.9.1 and justify your conclusions.

9.9.2 Run the MODFLOW model for the problem in Example 9.9.1 using a time step of one day and a time step multiplier of 1.0. Use an initial head condition of 1,000 ft in the active part of the grid. Compare the results with those obtained in Example 9.9.1 and justify your conclusions.

9.9.3 Run the MODFLOW model for the system in Example 9.9.1 in a transient mode. Five time steps are to be used with a time step multiplier of 1.5 and a stress period length of 365 days specified in the BASIC package. Print the mass balance (budget) and head distributions for all five time steps using the OUTPUT CONTROL PACKAGE. Use a specific storage of 0.01.

9.9.4 Modify the data set from Problem 9.9.3 to use the OUTPUT CONTROL PACKAGE to print out the model-wide mass balance and to save the cell-by-cell budgets for the BCF, WELL, and RECHARGE packages at time step 1. Use the hydraulic heads generated for time step 1 to manually compute the model-wide rate components into storage, out of storage, well discharge, out of constant heads, into constant heads, and recharge. Use Darcy's law to compute constant head flux. Also use the definition of the storage coefficient to determine the rate change in storage. Compare your results to those computed by the model.

9.9.5 Use the input file developed for Problem 9.9.4 and run it to obtain the cell-by-cell budgets. Compare the model-generated values to the Problem 9.9.4 hand calculations.

9.9.6 Use the model developed in Problem 9.9.1 and eliminate the well in row 5, column 3. Perform a steady-state simulation for a recharge of 0.001 ft/d and a transmissivity of 500 ft^2/d.

9.9.7 Use the model developed in Problem 9.9.1 and eliminate the well in row 5, column 3. Perform a steady-state simulation for a recharge of 0.001 ft/d and a transmissivity of 50 ft^2/d. Compare the hydraulic heads to those generated in Problem 9.9.6.

9.9.8 Use the model developed in Problem 9.9.1 and eliminate the well in row 5, column 3. Perform a steady-state simulation for a recharge of 0.0001 ft/d and a transmissivity of 50 ft^2/d. Compare the hydraulic heads to those generated in Problem 9.9.6.

9.9.9 Rerun the steady-state model (one stress period and one time step of one day) developed in Problem 9.9.6 with the option in the BCF package invoked to print out the individual specified head fluxes.

9.9.10 Run the steady-state model (one stress period and one time step of one day) developed in Problem 9.9.9 with a well in row 5, column 3 pumping at a rate of –8,000 ft^3/d. Print out the individual specified head fluxes and compare these to those generated in Problem 9.9.9.

9.9.11 Develop a drawdown model using the parameters and stresses of Problem 9.9.10. Use an initial head of 0.0, a recharge rate of 0.0, and specified heads of 0.0 along row one and column 7. Run the steady-state model with one stress period and one time step of one day, printing out the individual specified head fluxes. On a node-by-node basis, add the heads generated in Problem 9.9.9 and the solution generated in this problem. Compare these heads to those generated in Problem 9.9.10.

9.9.12 Resolve Problem 9.9.11 with the well rate doubled. Compare the heads of Problem 9.9.11 with those generated in this problem.

9.9.13 Resolve Example 9.9.2, doubling the transmissivity. All other data remain the same. Compare the results with those reported in Example 9.9.2.

9.9.14 Resolve Example 9.9.2 using a 30 by 30 grid. Compare the results with those presented in Example 9.9.2.

REFERENCES

1. Alley, W. M., T. E. Reilly, and O. L. Franke, *Sustainability of Ground-Water Resources, U.S. Geological Survey Circular* 1186, 1999.

2. Anderman, E. R., and M. C. Hill, *Advective-Transport Observation (ADV) Package, a Computer Program for Adding Advective-Transport Observations of Steady-State Flow Fields to the Three-Dimensional Ground-Water Flow Parameter-Estimation Nodel MODFLOWP, U.S. Geological Survey Open-File Report* 97-14, 67 pp, 1997.

3. Anderman, E. R., and M. C. Hill, *MODFLOW-2000, The U.S. Geological Survey Modular Groundwater Model—Documentation of the Hydrologeologic-Unit Flow (HUF) Package, U.S. Geological Survey Open-File Report* 00-342, 89 pp, 2000.

4. Anderson, M. P., and W. W. Woessner, *Applied Groundwater Modeling: Simulation of Flow and Advective Transport*, Academic Press, San Diego, CA, 1992.

5. Appel, C. A., and J. D. Bredehoeft, *Status of Groundwater Modeling in the U.S. Geological Survey, U.S. Geological Survey Circular* 737, 1976.

6. Banta, E. R., *MODFLOW-2000, The U.S. Geological Survey Modular Groundwater Model—Documentation of Packages for Simulating Evapotranspiration with a Segmented Function (ETS1) and Drains with Return Flow (DRT1), U.S. Geological Survey Open-File Report* 00-466, 127 pp, 2000.

7. Belitz, K., and S. P. Phillips, *Numerical Simulation of Ground-Water Flow in the Central Part of the Western San Joaquin Valley, California, U.S. Geological Survey Water-Supply Paper* 2396, 69 pp, 1993.

8. Buxton, H., and T. E. Reilly, *A Technique for Analysis of Ground-Water Systems of Regional and Subregional Scales Applied to Long Island, New York, U.S. Geological Survey Water-Supply Paper* 2310, pp. 129–142, 1986.

9. Chiang, W. H., and W. Kinzelbach, *3D-Groundwater Modeling with PMWIN, A Simulation System for Modeling Groundwater Flow and Pollution*, Springer, Berlin, 2000.

10. Fenske, J. P., S. A. Leake, and D. E. Prudic, *Documentation of a Computer Program (RES1) to Simulate Leakage from Reservoirs Using Modular Finite Difference Groundwater Flow Model (MODFLOW), U.S. Geological Survey Open-File Report* 96-364, 51 pp, 1996.

11. Freeze, R. A., and J. A. Cherry, *Groundwater*, Prentice Hall, Englewood Cliffs, NJ, 1979.

12. Goode, D. J., Particle velocity interpolation in block-centered finite difference groundwater flow models, *Water Resources Research*, v. 26, no. 5, pp. 925–940, 1990.

13. Goode, D. J., Age, *Double Porosity, and Simple Reaction Modifications for the MOC3D Ground-Water Transport Model, U.S. Geological Survey Water-Resources Investigations Report* 99-4041, 1999.

14. Goode, D. J., *Simulating Contaminant Attenuation, Double-Porosity Exchange, and Water Age in Aquifers Using MOC3D, U.S. Geological Survey Fact Sheet* 086-99, April 1999.

15. Goode, D. J., and C. A. Appel, *Finite Difference Interblock Transmissivity for Unconfined Aquifers and for Aquifers Having Smoothly Varying Transmissivity, U.S. Geological Survey Water-Resources Investigations Report* 92-4124, 79 pp, 1992.

16. Grubbs, J. W., *Evaluation of Ground-Water and Hydrologic Budget for Lake Five-O, a Seepage Lake in Northwestern Florida, U.S. Geological Survey, Water-Resources Investigations Report* 94-4145, Tallahassee, FL, 1995.

17. Hanson, R. T., and S. A. Leake, *Documentation for HYMOD, A Program for Extracting and Processing Time-Series Data from the U.S. Geological Survey's Modular Three-Dimensional Finite Difference Ground-Water Flow Model, U.S. Geological Survey Open-File Report* 98-564, 57 pp, 1999.

18. Harbaugh, A. W., *A Generalized Finite-Difference Interblock Transmissivity for Unconfined Aquifers and for Aquifers Having Smoothly Varying Transmissivity, U.S. Geological Survey Open-File Report* 91-494, 60 pp, 1992.

19. Harbaugh, A. W., *Direct Solution Package Based on Alternating Diagonal Ordering for the U.S. Geological Modular Finite-Difference Groundwater Flow Model, U.S. Geological Survey Open-File Report* 95-288, 46 pp, 1995.

20. Harbaugh, A. W., E. R. Banta, M. C. Hill, and M. G. McDonald, *MODFLOW-2000: The U.S. Geological Survey Modular Ground-Water Model—User Guide to Modularization Concepts and the Ground-Water Flow Process, U.S. Geological Survey Open-File Report* 00-92, 121 pp, Reston, VA, 2000.

21. Harbaugh, A. W., and M. G. McDonald, *User's Documentation for MODFLOW-96, An Update to the United States Geological Survey Modular Finite Difference Groundwater Flow Model, U.S. Geological Survey Open-File Report* 96-485, 56 pp, 1996.

22. Harbaugh, A. W., and M. G. McDonald, *Programmer's Documentation for MODFLOW-96, An Update to the U.S. Geological Modular Finite Difference Groundwater Flow Model, U.S. Geological Open File Report* 96-486, 220 pp, 1996.

23. Heberton, C. I., T. F. Russell, L. F. Konikow, and G. Z. Hornberger, *A Three-Dimensional Finite Volume Eulerian-Lagrangian Localized Adjoint Method (ELLAM) for Solute Transport Modeling, U.S. Geological Survey Water Resources Investigations Report* 00-4087, Reston, VA, 2000.

24. Hill, M. C., *Preconditioned Conjugate-Gradient 2 (PCG2), a Computer Program for Solving Ground-Water Flow Equations, U.S. Geological Survey Water-Resources Investigations Report* 90-4048, 43 pp, 1990.

25. Hill, M. C., *Methods and Guidelines for Effective Model Calibration, U.S. Geological Survey Water-Resources Investigations Report* 98-4005, 90 pp, 1998.

26. Hill, M. C., E. R. Banta, A. W. Harbaugh, and E. R. Anderman, *MODFLOW-2000, The U.S. Geological Survey Modular Ground-Water Model—User Guide to the Observation, Sensitivity, and Parameter-Estimation Processes and Three Post-Processing Programs, U.S. Geological Survey Open-File Report* 00-184, 210 pp, 2000.

27. Hornberger, G. Z., L. F. Konikow, and P. T. Harte, *Simulating Horizontal-Flow Barriers Using the MODFLOW Ground-Water Transport Process, U.S. Geological Survey Open-File Report* 02-52, 2002.

28. Hsieh, P. A., and J. R. Freckleton, *Documentation of a Computer Program to Simulate Horizontal-Flow Barriers Using the U.S. Geological Survey Modular Three-Dimensional Finite Difference Ground-Water Flow Model, U.S. Geological Survey Open-File Report* 92-477, 32 pp, 1993.

29. Kipp, K. L., L. F. Konikow, and G. Z. Hornberger, *An Implicit Dispersive Transport Algorithm for the U.S. Geological Survey MOC3D Solute-Transport Model, U.S. Geological Survey Water-Resources Investigations Report* 98-4234, 1998.

30. Klempt, W. B., T. R. Knowles, G. R. Elder, and T. W. Sieh, Groundwater Resources and Model Applications for the Edwards (Balcones Fault Zone) Aquifer in the San Antonio Region, Texas, Report 239, Texas Department of Water Resources, Austin, TX, October 1979.

31. Konikow, L. F., and J. D. Bredehoeft, Groundwater models cannot be validated, *Advances in Water Resources*, v. 15, pp. 75–83, 1992.

32. Konikow, L. F., D. J. Goode, and G. Z. Hornberger, *A Three-Dimensional Method-of-Characteristics Solute-Transport Model (MOC3D), U.S. Geological Survey Water Resources Investigations Report* 96-4267, 87 pp, 1996.

33. Landmeyer, J. E., F. H. Chapelle, P. M. Bradley, J. F. Pankow, C. D. Church, and P. G. Tratnyek, Fate of MTBE relative to benzene in a gasoline-contamination aquifer (1993–1998), *Ground Water Monitoring and Remediation*, v. 18, No. 4, pp. 93–102, 1998.

34. Leake, S. A., and D. V. Claar, *Procedures and Computer Programs for Telescopic Mesh Refinement Using MODFLOW, U.S. Geological Survey Open-File Report* 99-238, 53 pp, 1999.

35. Leake, S. A., and M. R. Lilly, *Documentation of a Computer Program (FHB1) for Assignment of Transient Specified-Flow and Specified-Head Boundaries in Applications of the Modular Finite Difference Groundwater Flow Model (MODFLOW), U.S. Geological Survey Open-File Report* 97-571, 50 pp, 1997.

36. Leake, S. A., and D. E. Prudic, *Documentation of a Computer Program to Simulate Aquifer-System Compaction Using the Modular Finite Difference Ground-Water Flow Model, U.S. Geological Survey Techniques of Water-Resources Investigations*, Book 6, Chap. A2, 68 pp, 1991.

37. Liggett, J. A., and P. L-F., Liu, *The Boundary Integral Equation Method for Porous Media Flow*, Allen and Unwin, 255 pp, 1983.

38. McDonald, J. M., and A. W. Harbaugh, *A Modular Three-Dimensional Finite Difference Groundwater Flow Model, U.S. Geological Survey Open-File Report* 83-875, 528 pp, 1984.

39. McDonald, J. M., and A. W. Harbaugh, A modular three-dimensional finite difference groundwater flow model, *Techniques of Water Resources Investigations of the United States Geological Survey*, Book 6, pp. 586, 1988.

40. McDonald, M. G., A. W. Harbaugh, B. R. Orr, and D. J. Ackerman, *A Method of Converting No-Flow Cells to Variable-Head Cells for the U.S. Geological Survey Finite Difference Groundwater Flow Model, U.S. Geological Survey Open-File Report* 91-536, 99 pp, 1992.

41. Merritt, M. L., and L. F. Konikow, *Documentation of a Computer Program to Simulate Lake-Aquifer Interaction Using MODFLOW Groundwater Flow Model and the MOC3D Solute-Transport Model, U.S. Geological Survey Water-Resources Investigations Report* 00-4167, 146 pp, 2000.

42. Miller, R. T., and C. I. Voss, Finite difference grid for a doublet well in an anisotropic aquifer, *Ground Water*, v. 24, no. 4, pp. 490–496, 1987.

43. Peaceman, D. W., *Fundamentals of Numerical Reservoir Simulation*, Elsevier Scientific Publishing Company, Oxford, UK, 1977.

44. Peaceman, D. W., and H. H. Rachford, Jr., The numerical solution of parabolic and elliptic differential equations, *Jour. Soc. of Industrial and Applied Mathematics*, v. 3, pp. 28–41, 1955.

45. Pinder, G. F., and W. G. Gray, *Finite Element Simulation in Surface and Subsurface Hydrology*, Academic Press, San Diego, CA, 295 pp, 1977.

46. Pollock, D. W., Semianalytical computation of path lines for finite difference models, *Ground Water*, v. 26, no. 6, pp. 743–750, 1988.

47. Pollock, D. W., *Documentation of Computer Programs to Compute and Display Pathlines Using Results from the U.S. Geological Survey Modular Three-Dimensional Finite-Difference Ground-Water Flow Model, U.S. Geological Survey Open-File Report* 89-381, 188 pp, 1989.

48. Pollock, D. W., *User's guide for MODPATH/MODPATH-PLOT, Version 3: A Particle Tracking Post-Processing Package for MODFLOW, the U.S. Geological Survey Finite-Difference Ground-Water Flow Model, U.S. Geological Survey Open-File Report* 94-464, 234 pp, 1994.

49. Prickett, T. A., Modeling techniques for groundwater evaluation, in V. T. Chow, ed., *Advances in Hydroscience*, Academic Press, v. 10, pp. 1–143, 1975.

50. Prickett, T. A., Ground-water computer models—State of the art, *Ground Water*, v. 17, pp. 167–173, 1979.

51. Prickett, T. A., and Lonnquist, C. G., Selected digital computer techniques for groundwater resources evaluation, *Bulletin No. 55*, Illinois State Water Survey, Urbana, IL, 1971.

52. Prince, K. R., O. L. Franke, and T. E. Reilly, *Quantitative Assessment of the Shallow Ground-Water Flow System Associated with Conneeetquot Brook, Long Island, New York, U.S. Geological Survey Water-Supply Paper* 2309, 28 pp, 1988.

53. Prudic, D. E., *Documentation of a Computer Program to Simulate Stream-Aquifer Relations Using a Modular, Finite-Difference, Groundwater Flow Model, U.S. Geological Survey Open-File Report* 88-729, 113 pp, 1989.

54. Remson, I., G. W. Hornberger, and F. J. Molz, *Numerical Methods in Subsurface Hydrology*, Wiley-Interscience, New York, 389 pp, 1971.

55. Rushton, K. R., and S. C. Redshaw, *Seepage and Groundwater Flow—Numerical Analysis by Analog and Digital Methods*, John Wiley & Sons, New York, 1979.

56. Texas Water Development Board, GWSIM groundwater simulation program, program document and user's manual, UM S7405, Austin, TX, 1974.

57. Todd, D. K., *Groundwater Hydrology*, 2nd ed., John Wiley & Sons, New York, 1980.

58. Trescott, P. C., G. F. Pinder, and S. P Larson, Finite-difference model for aquifer simulation in two dimensions with results of numerical experiments, in *U S. Geological Survey Techniques of Water Resources Investigations*, Book 7, C1, U.S. Geological Survey, Reston, VA, 1976.

59. Walton, W.C., *Groundwater Resource Evaluation*, McGraw-Hill, New York, 1970.

60. Walton, W. C., *Numerical Groundwater Modeling: Flow and Contaminant Migration*, Lewis Publishers, Boca Raton, FL, 272 pp, 1989.

61. Wanakule, N., *Optimal Groundwater Management Models for the Barton Springs-Edwards Aquifer*, Edwards Aquifer Research and Data Center, San Marcos, TX, 1989.

62. Wang, H. F., and M. P. Anderson, *Introduction to Groundwater Modeling: Finite Difference and Finite Element Models*, W. H. Freeman, San Francisco, CA, 1982.

63. Ward, D. S., D. R. Buss, J. W. Mercer, and S. S. Hughes, Evaluation of a groundwater corrective action at the Chem-Dyne hazardous waste site using telescope mesh refinement modeling approach, *Water Resources Research*, v. 23, no. 4, pp. 603–617, 1987.

64. Yeh, W. W. G., Groundwater Systems, Ch. 16, in *Water Resources Handbook*, L. W. Mays, ed., McGraw-Hill, New York, 1996.